Energy & Buildings 308 (2024) 114011

Contents lists available at ScienceDirect

Energy & Buildings

journal homepage: www.elsevier.com/locate/enb

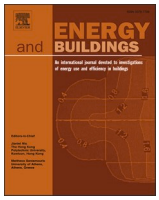

Dynamic building thermal mass clustering for energy flexibility assessment: An application to demand response events

Alice Mugnini [a,*], Alfonso P. Ramallo-González [b], Adelaida Parreño [c], Angel Molina-Garcia [b], Antonio F. Skarmeta [c], Alessia Arteconi [a,d]

[a] Dipartimento di Ingegneria Industriale e Scienze Matematiche, Università Politecnica delle Marche, Via Brecce Bianche 12, 60131, Ancona, Italy
[b] Department of Automatics, Electrical Engineering and Electronic Technology, Universidad Politécnica de Cartagena, 30202 Cartagena, Spain
[c] Department of Information and Communication Engineering, Universidad de Murcia, 30100 Murcia, Spain
[d] Department of Mechanical Engineering, KU Leuven, B-3000, Leuven, Belgium

ARTICLE INFO

Keywords:
Demand response
Dynamic energy flexibility
Building thermal mass
Building labelling
Lumped parameter model
Time constants

ABSTRACT

Demand response programs encompass a range of externally control strategies designed to modify consumer end-use load according to specific grid demands. In the current renewable integration context, power systems need to implement such demand strategies to provide energy flexibility during grid stress periods. Nevertheless, the extensive adoption of demand response initiatives in the building sector is confronted by notable obstacles, mainly due to the absence of standardized assessment methods and metrics, and the lack of established regulatory frameworks, all of which hinder the formation of competitive flexibility asset portfolios. Indeed, energy flexibility quantification frameworks are not unified and are usually based on the control objectives and quantification indicators. In this framework, this paper proposes a methodology to cluster residential buildings based on the analytical assessment of their dynamic thermal response, regardless the boundary conditions (i.e., weather data, occupancies, …) and the type of demand response event. The proposed methodology provides a quick and simple quantification of how a building is expected to respond under different demand response events and durations, which is critical for both customers and demand response agents to decide and select the involvement of buildings in each event and potentially to design personalized demand response events for each building.

An extensive analysis was conducted to evaluate the methodology based on 28 real residential buildings, whose data were presented in a previous study. Results provide the potential effectiveness and application for energy flexibility purposes of this methodology based on dynamic thermal building clustering. Moreover, it can be concluded that it is not possible to deduce a thermal inertia available classification exclusively based on design thermal and geometric characteristics of the building; being necessary to consider the duration of involvement, since they highly influence on the residential building thermal behavior, and thus, on the corresponding clustering.

1. Introduction

To cope with global warming and the forthcoming fossil fuel crisis, many countries, including the European Union [1], have committed to becoming NetZero by 2050 [2]. One of the main strategies to achieve the goal is the transition to an energy system based on renewable energy sources [3]. However, the unpredictable nature of the most common renewable sources, such as wind and solar resources, requires solutions to ensure the security of energy supply [4]. This point makes necessary to rethink the management of the entire energy system [5]. Moreover, the electrification of transportation is leading to increased demand peaks, potentially triggering inherent stability issues.

Whereas the traditional management involves tracking energy demand with generation, the new management will have to be able to adapt energy power to available generation (i.e., Demand Side Management, DSM [6]). DSM includes all strategies aimed at influencing energy consumption to optimize generation, distribution, and energy end use [7]. DSM strategies can be classified into energy efficiency and Demand Response (DR) [8]. Specifically, DR commonly provides

* Corresponding author.
E-mail addresses: a.mugnini@univpm.it (A. Mugnini), alfonsop.ramallo@upct.es (A.P. Ramallo-González), adelaida.parreno@um.es (A. Parreño), angel.molina@upct.es (A. Molina-Garcia), skarmeta@um.es (A.F. Skarmeta), a.arteconi@univpm.it (A. Arteconi).

https://doi.org/10.1016/j.enbuild.2024.114011
Received 8 November 2023; Received in revised form 29 January 2024; Accepted 15 February 2024
Available online 20 February 2024

Nomenclature

Acronyms

COP	Coefficient of Performance
DSM	Demand Side Management
DR	Demand Response
HVAC	Heating, Ventilation and Air Conditioning
ID	Building identifier
LPM	Lumped Parameter Model

Symbols

A	First thermal inertia class (high performance)
$\boldsymbol{A}$	System matrix state space formulation
B	Second thermal inertia class (medium–high performance)
$\boldsymbol{B}$	Input matrix state space formulation
C	Heat capacitors (Wh/K)
C	Third thermal inertia class (medium–low performance)
$\boldsymbol{C}$	Output matrix state space formulation
D	Forth thermal inertia class (low performance)
$\boldsymbol{D}$	Feedthrough matrix state space formulation
f	Factor (-)
q	Heat power (W)
R	Thermal resistance (K/W)
t	Time (hours)
T	Temperature (°C)
$\boldsymbol{U}$	Input vector
$\boldsymbol{X}$	State vector
$\boldsymbol{Y}$	Output vector
τ	Time constant (hours)

Subscripts

i	referred to the internal air node
TM	referred to the virtual node representing the internal thermal mass
e	referred to electrical gains
HVAC	referred to the Heating, Ventilation and Air Conditioning
L	referred to long-time events
s	referred to solar gains
S	referred to short-time events
w	referred to the virtual temperature of the interior of the thermal envelope

incentives to shift or reduce demand in electricity markets to balance the grid [9]. Subsequently, promoting the large-scale application of DR strategies can have a considerable impact on the flexibility of the systems under a high penetration of renewables [10].

In this context, the building sector can play a key role [11]. There are many reasons why buildings can contribute significantly to the energy transition. Firstly, their impact on the overall energy demand. In fact, and according to the International Energy Agency, buildings are responsible for about 30 % of global final energy consumption [12]. Secondly, there is plenty of space for energy efficiency. For example, considering the European Union, it is estimated that around 75 % of buildings need major renovation [13], and at least 60 % of the buildings heat demand worldwide are still met by fossil fuels [14]. Moreover, buildings allow to decouple rather easily demand for heating and/or cooling from generation. Indeed, different thermal inertia reserves can be exploited in buildings [15]. For instance, the thermal mass of the envelope can be used as a storage medium [16], the thermostat can be controlled with a temperature dead band (e.g., by exploiting thermostatically controllable loads [17]), or heating and/or cooling systems can be equipped with external storage devices (sensible [18] or latent [19] thermal energy storage systems). Finally, the increasing spread of high-efficiency electrically powered heating and cooling systems, such as electrically driven heat pumps, makes possible to directly link the manageable heat demand to the electricity consumption [20].

DSM programs, and especially DR events, can be successfully applied in buildings to provide grid flexibility [21]. Several pilot projects have already demonstrated this potential for applying DR event in buildings [22]. An energy flexible building is defined as a building able to manage its demand and/or generation according to local climatic conditions, user needs and energy grid requirements [23]. In general, how flexible a building depends on its intrinsic characteristics. In fact, both the geometry, the thermal losses, the thermal inertia of the envelope and the type of heating and/or cooling system are factors that determine how much heating/cooling demand can be decoupled from generation [24].

The above-mentioned factors contribute significantly to the energy efficiency of the building. However, unlike the efficiency, the quantification of a flexibility reserve is also highly dependent on the operation (i.e., the type of DR event, dynamically varying boundary conditions and the thermal dynamics of the building itself) [25]. For these reasons, the identification of a standard methodology for characterizing energy flexibility in buildings is still an open topic. However, if DR strategies are to be applied on a large scale, it is necessary for the DR agent, in charge of deciding on the activation of the energy flexibility of individual buildings, to be able to assess a priori which buildings are to be activated based on the different requirements of the grid. Therefore, a standard method to label buildings based on their response to different types of DR events is required. In fact, as Pallonetto *et al.* [26] also pointed out, currently the lack of commonly accepted and standardized metrics to assess DR represents one of the main obstacles to achieving a widespread distribution of DR programs in residential buildings.

Nowadays, recent contributions propose methodologies to quantify energy flexibility in buildings [27 28]. For instance, Junker *et al* [29] proposed a characterization of the energy flexibility of a building through a dynamic function (i.e., the Flexibility Function) and a Flexibility Index. The methodology is based on applying penalty signals to the building (e.g., price signal, CO_2 intensity or a control signal imposed by the grid) within penalty-aware control. Then flexibility index describes how the building dynamically reacts to the specific penalty signal. Majdalani *et al.* [30] evaluated energy flexibility such as the ability of the building to respond to a cost signal. In particular, the authors proposed a single indicator (i.e., the Expected Flexibility Savings Index) to assess the energy flexibility obtainable from the management of heating and cooling systems in residential buildings. Arteconi *et al.* [24] also quantified flexibility with a single dimensionless indicator (i.e., the Flexibility Performance Indicator). In this case, however, the Flexibility Performance Indicator considers several aspects such as response and recovery time, power and shiftable energy. This study also showed how the indicator could be used to classify the potential flexibility reserve of the building during a standard DR event. On the other hand, Reynders *et al.* [31] introduced three flexibility indices to characterize different dimensions of the flexibility (i.e., size, time and cost). The performance indicators were: the available storage capacity, the storage efficiency and the power shifting capability. These were calculated by comparing the building heat power demand in the baseline scenario (i.e., without activation of flexibility) with the flexible scenario (i.e., in case of application of a single reference DR event). Tang and Wang [32] introduced two sets of flexibility indexes (i.e., flexibility capacities and flexibility ratios) to characterize the flexible response of buildings during DR events. In this case the methodology was based on the comparison between a flexible and a baseline scenario. Another study in which the potential reserve of energy flexibility was assessed through multiple indicators was conducted by Ruan *et al.* [33]. Here the authors

introduced three indicators representing energy efficiency, load and energy reduction. The indicators were calculated by comparing the results of dynamic simulations of the building without and with the application of a reference DR event. Extending the latter approach, Chena *et al.* [34] proposed different indicators according to the source of flexibility. Indeed, based on previous studies, the authors proposed a framework for energy flexibility quantification distinguishing among the following contributions: the energy generation from the building itself (e.g., PV panels on site), the building thermal mass, the contribution of dedicated storage devices and the shift loads ability of appliances. A different approach was presented by Li and Hong [35]. Indeed, Li and Hong proposed a data driven method to quantify energy flexibility in buildings. In this way, the authors did not need a baseline scenario to calculate the flexibility indicators but identified it from measured data of real buildings subjected to DSM programs. A similar approach was also proposed by Zhu *et al.* [36]. The authors developed a data-driven model to quantify the DR potential of building HVAC (Heating, Ventilation and Air Conditioning) systems. In particular, Zhu *et al.* introduced flexibility indicators, identified from the data, calculated on the basis of the generalization of the building response under different boundary conditions.

Recently, Lu *et al.* [37] affirmed that energy flexibility quantification frameworks are not unified and are usually based on the control objectives and quantification indicators. Based on the specific literature, most quantification methods consider flexibility as a property of the overall system (understood as the result of the actual interaction between the HVAC system and the grid). This assumption makes the estimation of the flexibility reserve dependent on the characteristics of each specific case study. On the other hand, few studies propose a method capable of analytically quantifying the thermal mass actually available in the building, regardless of the boundary conditions and the specific DR event.

Some of the studies characterizing energy flexibility in individual buildings are summarized in Table 1. Note that those mentioned are not all the available contributions on this topic, as the extensive scientific literature described in [27 28]. However, they represent some significant examples useful to distinguish the various characteristics of the available methodologies. Regarding Table 1, it can be observed that, in most cases the focus of the characterization is on the building, while the DR event is considered a reference condition. Furthermore, the energy flexibility is usually quantified and described as an intrinsic characteristic of the building, strongly related to the specific boundary conditions (i.e., the dynamic variation of weather conditions, the setpoint profile for comfort, …) and the type of DR event. Therefore, the most common flexibility indicators do not allow a direct evaluation of the thermal mass exploitable alone. On the contrary, they tend to aggregate and summarize the flexible behavior considering all dimensions of flexibility. However, from the point of view of a DR agent, it would be desirable to know how each building may respond according to a specific DR event and the current thermal mass available. In other words, it can be interpreted as a need to quantify the different levels of effective thermal inertia exploitable in a building. From this perspective, there is a lack of contributions and methods focused on labeling buildings based on their current thermal mass. To overcome this drawback, in this paper, the authors introduce a novel methodology that challenges the conventional approach used for categorizing energy flexibility in buildings (Table 1). Indeed, it is known that when a DR event is applied to an HVAC system in a building, its response changes significantly depending on the current thermal mass available and the type of DR event. In general, this thermal mass may not match with the entire thermal mass of the building and, furthermore, the same building may behave in a different way depending on the duration of the involvement (short events, e.g., a few minutes, or long events, e.g., hours). For these reasons, the thermal mass quantification is not able to be estimated directly from thermal and geometric characteristic estimations of the building; being highly dependent on the DR event itself. Under the present framework, quickly and simply quantifying how a building is expected to respond under different DR events is critical for DR agents. Consequently, the proposed methodology can be applied under both operational and planning DR scenarios, where it is crucial to decide and select the involvement of buildings in each DR event. The proposed methodology allows to characterize analytically the dynamic response of buildings, regardless of the boundary conditions (i.e., weather dynamics, season, role of occupants) and the type of DR event. In this way, a DR agent can have a general characterization of its available portfolio and plan involvement scenarios. Given the dynamic nature of assessing energy flexibility in buildings, the methodology is based on the thermal characterization of the dynamic response of the building; hence, a dynamic simulation model is required. The proposed methodology involves the calculation of two performance indicators (that could be considered as characteristic time constants) that allow to simplify the evaluation of how the building behaves during short- and long-term involvements. Based on the time constants, buildings can be labeled according to classes of current thermal inertia and thus facilitate the planning of building involvement scenarios by a DR agent. Furthermore, to show its potential in a more operational context, the methodology is also presented in two ways. Indeed, the labeling could be carried out both by considering only the building (i.e. independently of the specific boundary conditions such as the dynamics of the meteorological conditions and the imposed comfort condition) and from an operational perspective (i.e. considering all or some of the boundary conditions).

The rest of the paper is structured as follows: in Section 2 the methodology is described. The methodology contains the description of the dynamic model to be built and the procedures to be followed to calculate time constants and to identify labelling classes. Section 3 describes the case study. The results are presented and discussed in Section

Table 1
Overview of the mentioned methodologies to quantify energy flexibility of buildings during DR events.

Reference	Characterization through			Flexibility activation		Dependence on at least one boundary condition	Performance indicators differentiated by type of DR
	Dynamic function	Global indicator	Multiple indicators	Penalty-aware control	Simulation of a DR reference events		
Junker *et al* [29]	X	X		X		Yes	No
Majdalani *et al.* [30]	X	X		X		Yes	No
Arteconi *et al.* [24]		X			X	Yes	No
Reynders *et al.* [31]			X		X	Yes	No
Tang and Wang [32]			X		X	Yes	No
Ruan *et al.* [33]			X		X	Yes	No
Chen *et al.* [34]			X		X	Yes	No
Li and Hong [35]		X			X	Yes	No
Zhu *et al.* [36]		X			X	Yes	No
Methodology proposed in this study			X		X	No	Yes

4. Finally, the main conclusions are summarized in Section 5.

2. Methodology

This section describes the methodology to label buildings according to their current thermal mass. The responsiveness of a building during a DR event depends on both the intrinsic characteristics of the building (i.e., its thermal and geometric properties) and the type of DR event (i.e., type of DR signal and duration of involvement); but also, on the operational conditions of the building (i.e., its actual thermal dynamics and variable boundary conditions). For this reason, a Lumped Parameter Model (LPM) is identified for each building. Details concerning LPMs are described in Section 2.1. After the LPM definition, the dynamic response can be characterized by calculating the two proposed indicators: two characteristic time constants that allow a quick assessment of the ability of the building to respond under short- and long-term DR events. The two characteristic time constants differ from the traditional global time constant of the building [38], usually based on building design characteristics (i.e., thermal capacity of the building materials and thermal transmittance of the walls) and providing an averaged global thermal mass of the building. Instead, the time constants proposed in this work allow to quantify the current thermal mass available during different duration DR events. Furthermore, their calculation is based on LPMs. Therefore, they consider the real dynamic evolution of the building.

The proposed methodology is described in the most general form, aiming to be versatile for different case studies and classification objectives. In fact, characteristic time constants may (or may not) consider various aspects (i.e., boundary conditions) that, in any case, should be specified prior. As a summary, Fig. 1 shows schematically the proposed methodology.

2.1. Lumped parameter model identification

The selected LPM is based on equivalent resistors and thermal capacitances (RC-network). In fact, it is one of the most adopted solutions for thermal building modeling [39]. It can be identified both with measured data (i.e., grey box approach [40]) or obtained exclusively from knowledge of the thermal and geometric characteristics of the building (i.e., white box approach [41]). A third-order model is selected, being proposed by the specific literature as a suitable trade-off between computational effort and reliability [42 43]. Fig. 2 depicts a general scheme of the proposed LPM model. R_1, R_2, R_3, and R_4 are thermal resistances (in K/W), C_1, C_2 and C_3 are heat capacitors (in Wh/K), T_o is the outdoor air temperature (in °C), T_w is a virtual temperature of the interior of the thermal envelope (in °C), T_i is the temperature of the internal air (in °C), T_{TM} is the temperature of a virtual node modeling the internal thermal mass of the building (in °C), q_{HVAC} represents the heating or cooling output provided by the HVAC system (in W) and q_e, q_s are the electrical and solar gains (in W). The solar gains q_s are obtained from the total incident solar radiation, multiplied by a solar factor (f_S).

Eqs (1)–(3) describe the energy balance between nodes in the LPM:

$$C_1\frac{dT_w}{dt} = \frac{(T_o - T_w)}{R_1} + \frac{(T_i - T_w)}{R_2} \tag{1}$$

$$C_2\frac{dT_i}{dt} = \frac{(T_o - T_i)}{R_4} + \frac{(T_w - T_i)}{R_2} + \frac{(T_{TM} - T_i)}{R_3} + q_e + q_s + q_{HVAC} \tag{2}$$

$$C_3\frac{dT_{TM}}{dt} = \frac{(T_i - T_{TM})}{R_3} \tag{3}$$

Furthermore, with this formulation the LPM can be expressed in the form of a state space model according to Eqs. (4) and (5):

$$\dot{\boldsymbol{X}}(t) = \boldsymbol{A} \bullet \boldsymbol{X}(t) + \boldsymbol{B} \bullet \boldsymbol{U}(t) \tag{4}$$

$$\boldsymbol{Y}(t) = \boldsymbol{C} \bullet \boldsymbol{X}(t) + \boldsymbol{D} \bullet \boldsymbol{U}(t) \tag{5}$$

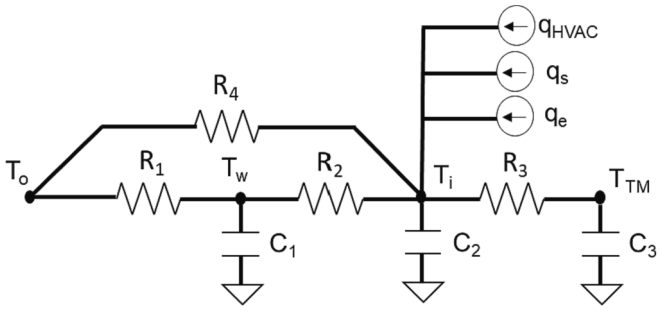

Fig. 2. LPM model (RC-network) [43].

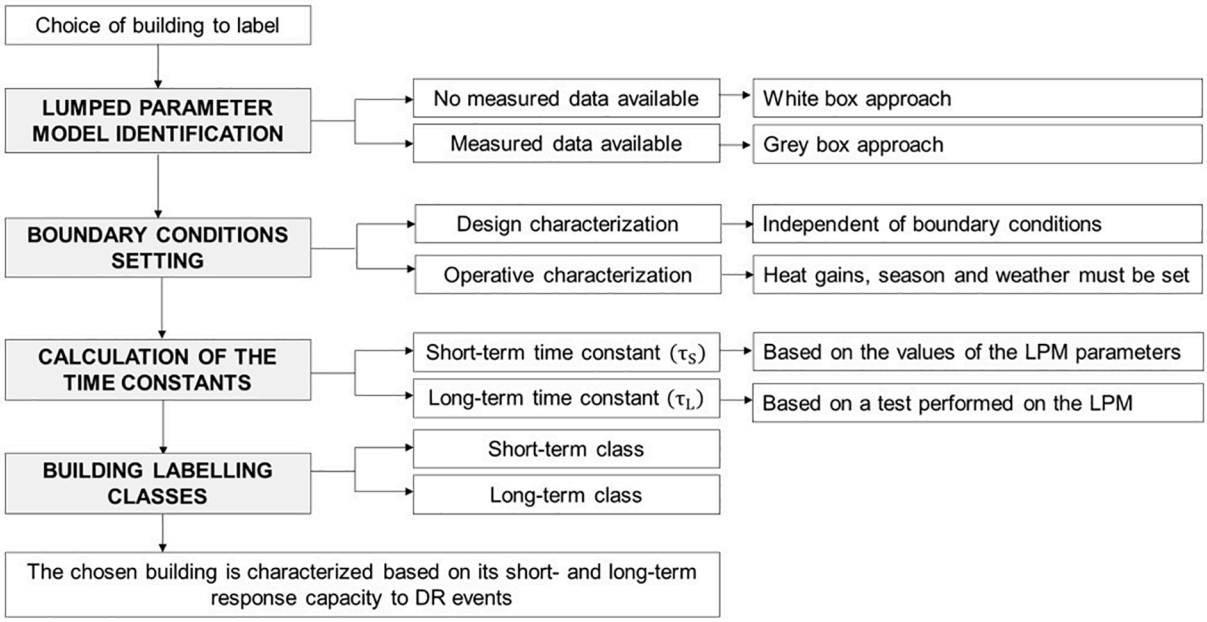

Fig. 1. General overview of the proposed methodology.

where $\boldsymbol{A}$, $\boldsymbol{B}$, $\boldsymbol{C}$ and $\mathbf{D}$ are respectively the system, the input, the output matrix, and feedthrough matrixes, $\dot{\boldsymbol{X}}(t)$ represents the state vector $\boldsymbol{U}(t)$ the input vector and $\boldsymbol{Y}(t)$ the output vector.

To better represent the dynamics of the building with a third order LPM, the authors suggest obtaining numerical values of the parameters (i.e., R_1, R_2, R_3, R_4, C_1, C_2 C_3 and f_S) with a grey box approach (i.e., see Annex A for more details). In the absence of measured data, a white box approach can also be used. However, it is important to point out that, even in the case of a white box approach, the key characteristics of the building (i.e., the geometric and thermal properties) must be known in advance. In any case, the current thermal inertia that is considered by the characterization methodology proposed in this study considers the information used to identify the LPM.

2.2. Boundary conditions settings

Time constants can be calculated for different characterization objectives. Indeed, they can be determined only considering the intrinsic characteristics of the building (i.e., design characterization). In this case, no boundary conditions are required, and the characterization of the building is suitable regardless of the season (i.e., heating or cooling) and location. The design characterization allows to consider only the intrinsic design features of the building, i.e., the geometry, the stratigraphy of the envelope walls, the type of fixtures, etc. On the other hand, the methodology can be applied also considering boundary conditions (i.e., operative characterization) and, in particular, heat gains. The definition of heat gains becomes the indicators representative for the building in those boundary conditions. As internal gains contribute differently depending on the season (reducing heating demand in winter and increasing cooling consumption in summer), it is essential to establish the following boundary conditions: (i) the season (whether it is heating or cooling), (ii) indoor comfort settings (the desired indoor thermostat temperature), and (iii) weather conditions (outdoor air temperature and overall solar irradiation). Regarding the operational characterization, time constants, can assume greater importance in assessing the individual building influence, or clusters of buildings, for different geographical locations and seasons.

2.3. Calculation of the time constants

Two indicators are introduced to characterize the current thermal inertia of a building. Both indicators have time dimension (i.e., expressed in hours) and allow to estimate the speed of the internal temperature changes respectively: (i) for the short-term (τ_S) and (ii) for the long-term response of the building (τ_L). Before defining τ_S and τ_L, it is necessary to stablish the initial assumptions to apply the methodology. With this aim, both boundary and the starting condition must be selected. These parameters include the outdoor temperature (T_o), the heat gains (q_e and q_s), the HVAC system contribution (q_{HVAC}) and the starting values of the states in LPM ($T_i(0), T_{TM}(0)$ and $T_w(0)$).

As described in the previous subsection, the definition of boundary conditions depends on the objective of the characterization. The following assumptions can be thus considered for design characterization purposes: (i) Fixed outdoor air temperature, although the numerical values of the time constants are not dependent on the numerical value of T_o. (ii) No contributions from heat gains due to electrical loads and solar radiation. (iii) Indoor air reference temperature ($T_{setpoint}$). Note that the numerical value of the parameter does not affect the time constants, and it does not take on the same numerical value as T_o. Moreover, such assumptions allow for a characterization independent of boundary conditions.

As far as the operative characterization is concerned, the above-mentioned variables are defined based on the specific case study. The outdoor temperature must be representative of the chosen location. The heat gains (q_e and q_s) are defined consistent with the location and case study, and the indoor air temperature setpoints ($T_{setpoint}$) must be defined according to the season under consideration (i.e., heating or cooling season). Note that only (iii) applies to both design and operational characterization.

Considering the initial values of the LPM states, such values can be defined from the test hypotheses according to:

$$T_i(0) = T_{TM}(0) = T_{setpoint} \tag{6}$$

$$T_w(0) = \frac{\frac{K_1 T_o}{R_1} + \frac{K_2 T_i(0)}{R_2}}{\frac{1}{R_1} + \frac{1}{R_2}} \tag{7}$$

As was previously discussed, the current thermal inertia of the building is characterized through the estimation of two characteristic time constants. These constants represent the DR response capacity of the building in the short (τ_S) and long term (τ_L). More specifically, they quantify how long the internal air temperature varies in comparison to ordinary indoor air temperature evolution, in the absence of DR events, differentiating short and longer observation time intervals. Their theoretical definitions are:

- τ_S: time interval in which the indoor air temperature (T_i) reaches 63.2 % of the maximum temperature difference ($T_o - T_{setpoint}$) at the growth rate defined by the first derivative at t equal to 0 hr. It can be analytically determined from the numerical values of the LPM parameters, see Fig. 2:

$$\tau_S = 0.632 \bullet C_2 \left(\frac{\frac{1}{R_1} + \frac{1}{R_2}}{\frac{1}{R_1 R_2} + \frac{1}{R_1 R_4} + \frac{1}{R_2 R_4}} \right) \tag{8}$$

- τ_L: time interval in which the indoor air temperature (T_i) reaches 63.2 % of the maximum temperature difference ($T_o - T_{setpoint}$), considering only the thermal mass of the building facing outwards. It is empirically determined by running the building model test. This test is carried out by setting the reciprocal of R_3 equal to 0 W K^{-1}. Fig. 3 shows the LPM used to calculate τ_L distinguishing between the characterization objective.

Note that a model suitable of representing the real processes need to find a trade-off between fidelity and number of parameters. When the number of parameters is too large, two issues can arise: (i) the overfitting, when the model is fitting only the data to be used for training and it probably would provide inconsistent results when extrapolating and (ii) the lack of identifiability when the combination of the parameters of the model can be high and produce the same answer. This last case is particularly treacherous for the objective of this study, hence the choice of a second order model and two-time constants to characterize the current thermal mass.

2.4. Building labeling classes

Based on the values obtained for the time constants (τ_S and τ_L), several differences among current thermal inertia classes can be then identified. In particular, the time constant τ_S allows to label the building in a short-term inertia class (identified with the subscript '*S*' in Fig. 4a). The time constant τ_L identifies the long-term inertia class (subscript '*L*' in Fig. 4b). The difference between these two inertia classes allows to identify dynamically such thermal mass able to be used in different duration DR events. The thresholds of the numerical values of the time constants that allow the classes in Fig. 4 to be divided can be deduced empirically from the comparison of the application of the methodology to multiple buildings. The numerical values of the time constants that allow the division of classes are obtained by clustering the results of the application of the methodology to several buildings. An example of

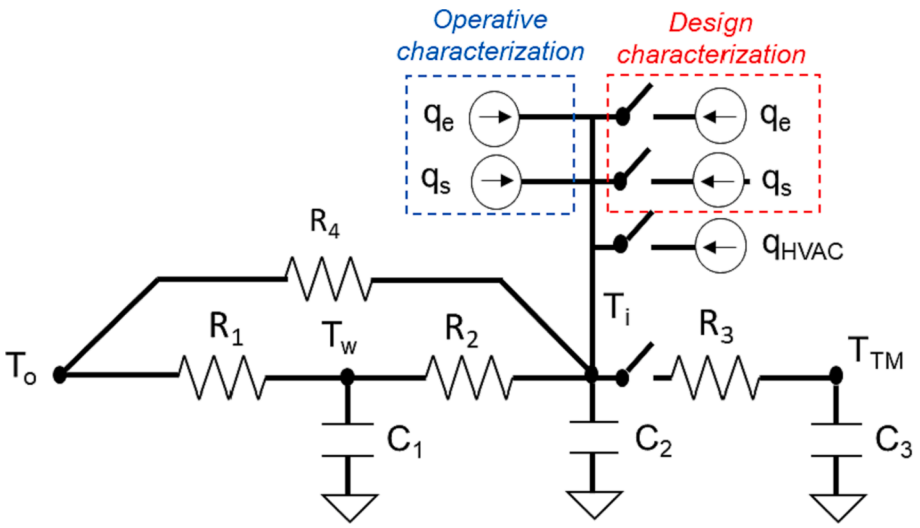

Fig. 3. LPM model to calculate τ_L: (design and operative characterization).

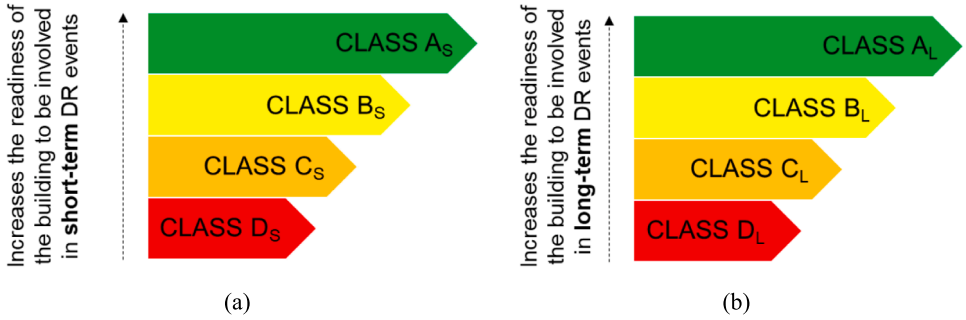

Fig. 4. Labeling of buildings based on their ability to respond to DR events: (a) classes for short term DR events and (b) classes for long-term DR events.

subdivision is shown in the following section, where a case study is introduced. In general, the definition of classes may be adaptable and modifiable. Indeed, each DR agent could apply the methodology to their own portfolio of buildings, thus establishing its own effective thermal inertia classes.

3. Case study

To assess the suitability of the proposed methodology, time constants are estimated for a case study composed of 28 real buildings. The case study was extensively described by the authors in [43], where also detailed numerical parameters of the LPMs are provided. However, for ease of reading, the main features of the case study are briefly described (for more details refer to [43]). Table 2 contains the main characteristics of the buildings. As can be seen, the portfolio is rather heterogeneous. In fact, the case study includes residential buildings which differ in terms of construction period (i.e., construction materials, stratigraphy, heat loss to the outside, type of windows, …), size, geometry, and type of building (i.e., mid terrace, detached cottage, semidetached, end terrace, …). Fig. 5 shows the heterogeneity of the case study, considering two representative parameters: (i) building size, assessed in terms of floor area in Fig. 5a; and (ii) building type in Fig. 5b.

Given the availability of measured data ([44]), a grey box approach was used to identify numerical values of the parameter for LPMs (Fig. 2). In particular, the dataset used for training contains time series of indoor temperature, outdoor temperature, and electricity consumption for each of the 28 buildings at 5-minute intervals. The fitting was very satisfactory. Indeed, the average error, calculated with respect to the cooling degree hours, showed an average error of 4.2 % and a worst-case difference of 13 % (Annex A for more details).

Both design and operative characterization were applied to the case study. In the former case, as described in the previous section, it was not necessary to choose a specific location for the calculation of time constants. However, to demonstrate the effectiveness of the design method and validate its classification, ideal DR events are applied to individual LPMs. The DR event consists of forced switching off the HVAC system when the peak power occurs. In one case, the forced shutdown is imposed for a short time interval (i.e., 5 min to assess the short-term responsiveness of the building). In the other case, the shutdown is imposed for a longer period (i.e., 2 h to assess long-term DR events). It is worth underlining that the definition of such DR events is only necessary to demonstrate the effectiveness of the methodology. The characterization results do not vary under different DR events. Summer season is considered, and meteorological data (data measured by the weather station) from the city of Murcia (N 37°59′-O 1° 7′, Spain) are used to estimate HVAC demand. The thermal power provided by the HVAC system is obtained by solving a linear programming optimization problem for each building [45]. The objective function of each optimization problem concerns the minimization of the thermal energy to maintain the internal temperature setpoint. In fact, the constraint conditions involve the state space equations (Eq. (1)-(3)) and require the internal temperature to remain close to the comfort set point. The cooling power of the HVAC (q_{HVAC} in Fig. 2) represents the decision variable. It is limited, to each time interval, by the maximum capability of the cooling system. The latter is represented by a real air–water heat pump. The rated power of each heat pump is calculated from the values of the heat loss coefficients given in Table 2 (a set-point comfort conditions of 24 °C is considered; i.e., $T_{setpoint}$ and the maximum reached

Table 2
Main characteristics of the case study buildings (ID assignment for each building) [43].

ID	Floor Area (sqm)	Type of building	Age of construction	Heat Losses (W/K)
1	31.2	3rd floor of Mid Terrace	1904	371.0
2	85	Mid Terrace	2006	114.0
3	85	Mid Terrace	2006	114.0
4	85	Mid Terrace	2006	114.0
5	93.91	Detached Cottage	1790	305.4
6	90.26	Semi Detached	1957	361.2
7	77.17	End Terrace	1959	279.6
8	65.62	Semi Detached	1924	363.7
9	64.86	3rd floor of Mid Terrace	1904	209.7
10	61.33	Semi Detached	1969	382.3
11	94.06	Semi Detached	2005	449.1
12	88	End Terrace	1964	245.6
13	57.22	Mid Terrace	1904	284.4
14	88.8	End Terrace	1960	231.9
15	95.81	End Terrace	2005	134.2
16	77.8	Semi Detached	1964	237.2
17	62.52	End Terrace	1969	223.3
18	95.81	Mid Terrace	2005	134.2
19	67.27	3rd floor of Mid Terrace	1904	237.1
20	58.85	Mid Terrace	1969	212.3
21	95.81	End Terrace	2005	134.2
22	95.81	End Terrace	2005	134.2
23	75.63	Terrace	1969	230.6
24	38.66	Mid Terrace	1904	260.4
25	95.81	End Terrace	2005	134.2
26	41.8	Semi Detached	1970	140.7
27	77.17	Mid Terrace	1969	270.7
28	80.9	End Terrace	1959	322.1

outdoor temperature of 45 °C). To obtain electricity consumption, the dynamic variation of the Coefficient of Performance (COP) with the operational condition (i.e., modulation, source and sink temperatures) are modeled by linear interpolation of the data provided by the manufacturer (a fixed water supply temperature of 7 °C is assumed) [45]. Table 3 summarizes the rated cooling loads for each building and the rated power of the corresponding heat pump (COP at full load, outdoor air temperature of 45 °C and water supply of 7 °C equal to 2.16).

Regarding the operative classification of the case study, reference values for q_s are used, see Fig. 3. The reference values are extrapolated from the classification of European climates conducted by Pernigotto and Gasparella [46]. In that work, the authors presented a new classification of 66 European climates based on clustering analysis. They identified six representative climate zones based on similar conditions of dry bulb temperature, relative humidity and global horizontal irradiation. For each climate zone, representative cities were identified as summarized Table 4.

Considering that the contribution of solar gains is not constant, its influence depending on the operating mode of the HVAC system (i.e., heating or cooling), two solar irradiation values are assessed for each location (one for winter and one for summer). These values are kept constant and applied as inputs to the LPM in Fig. 3. In detail, $q_{s,winter}$ (in W m^{-2}) is calculated as the average daily equivalent solar irradiation during winter (calculated considering the months of December, January and February). In a similar way, $q_{s,summer}$ (W m^{-2}) is assumed as the average daily equivalent solar irradiation during summer (calculated with reference to the months of July and August). These values were considered by considering representative typical meteorological year (TMY) for the representative cities in Table 5 [47].

In addition, the time constants under the presence of heat gains depend on the values of the outdoor air temperature and the starting

Table 3
Rated cooling load and side of the heat pump for each case study buildings (ID assignment for each building).

ID	Rated cooling loads (W/ m^{-2}(−|-))	Heat Pump cooling capacity (Water 7 °C/ Air 45 °C) (kW)
1	249.7	7.8
2	28.2	2.4
3	28.2	2.4
4	28.2	2.4
5	68.3	6.4
6	84.0	7.6
7	76.1	5.9
8	116.4	7.6
9	67.9	4.4
10	130.9	8.0
11	100.3	9.4
12	58.6	5.2
13	104.4	6.0
14	54.8	4.9
15	29.4	2.8
16	64.0	5.0
17	75.0	4.7
18	29.4	2.8
19	74.0	5.0
20	75.8	4.5
21	29.4	2.8
22	29.4	2.8
23	64.0	4.8
24	141.4	5.5
25	29.4	2.8
26	70.7	3.0

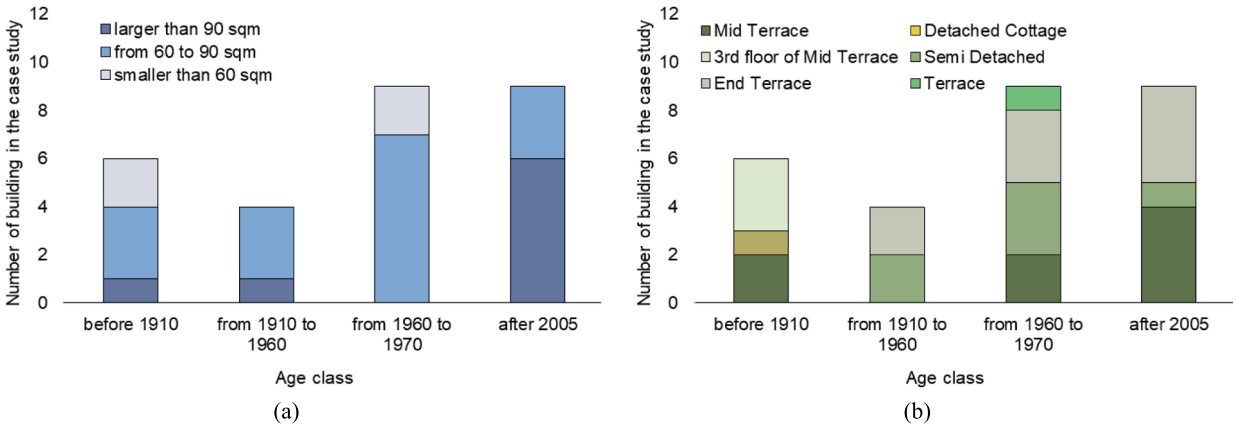

Fig. 5. Case study composition: (a) distinction according to construction period and building size (floor area) and (b) distinction according to construction period and building type.

Table 4
European climatic zones [46].

Climatic zone	Description	Representative city
1	Cold climate without dry season and with cold summer	Ostersund (Sweden)
2	Cold climate without dry season and with warm summer	Prague, Ostrava (Czech Republic) or Poznan (Poland)
3	Temperate climate without dry season and with warm summer	Strasbourg (France)
4	Temperate climate with dry and hot summer	Marseille (France)
5	Temperate climate without dry season and with hot summer	Pescara (Italy).
6	Temperate climate with dry and hot summer	Sevilla (Spain), Messina (Italy) or Larnaca (Cyprus)

Table 5
Reference solar irradiation values for each European climatic zone.

Climatic zone	$q_{s,winter}$ ($W/m^{-2}(-\|-)$)	$q_{s,summer}$ ($W/m^{-2}(-\|-)$)
1	59	250
2	117	316
3	122	370
4	208	461
5	201	437
6	275	513

value of the indoor air temperature. However, to evaluate only the contribution of the solar gains, the fixed outdoor temperatures of 40 °C and 0 °C (T_o) are assumed for all climate zones, for summer and winter seasons respectively. The initial conditions for indoor air were 24 °C and 20 °C for comfort in summer and comfort in winter ($T_{setpoint}$) accordingly. Again, as for the DR events tested, these values are chosen only to show with a practical case the effectiveness of the building categorization methodology. In particular, the choice to keep the outdoor temperatures fixed is made only to highlight the role of solar gains. Additional tests could be performed by users who want to apply the methodology to highlight the impact of other boundary conditions in the operative classification.

4. Results

In this section, the results of applying the proposed methodology to the case study are described and discussed. In particular, the first subsection (4.1) describes the design characterization and the division into classes of current thermal inertia. The second subsection (4.2) gives the operative characterization. Finally, in the last subsection (4.3), it is clarified how the proposed methodology ca be used by a DR agent. In this last subsection, the strengths and limitations of the methodology are also discussed.

4.1. Design characterization

This subsection describes the application of the design characterization methodology to the 28 buildings previously described in Section 3. Firstly, the performance indicators (i.e., τ_S and τ_L) and the division of the buildings into current inertia classes is reported. Secondly, DR events are applied to the LPMs of each building aimed to validate the proposed methodology.

4.1.1. Calculation of time constants for design characterization

The estimated time constants for all 28 buildings shown in the case study are summarized in Table 6. By considering the relevant variability of time constants among the different buildings, a traditional clustering algorithm (i.e., K-means clustering) is applied to classify such buildings according to their short- and long-term response with this we intend to verify if the buildings can be indeed classified in clusters, see Fig. 6. Two divisions of clusters are identified: the short-term time constant (see τ_S in Fig. 6a) and the longer-term time constant (see τ_L in Fig. 6b). Tables 7 and 8 give the list of buildings enclosed in each cluster for short-term response (Table 7) and for long-term response (Table 8) respectively.

Table 6
Time constants (design characterization).

BULDING ID	τ_S(hr)	τ_L(hr)
1	1.0	1.7
2	1.3	2.1
3	3.1	4.9
4	1.5	2.4
5	1.1	1.8
6	0.8	1.7
7	1.2	2.1
8	1.2	2.1
9	1.6	2.6
10	1.3	2.2
11	1.0	2.2
12	0.8	1.7
13	1.9	3.0
14	1.6	2.7
15	0.5	2.5
16	1.5	2.8
17	2.0	3.3
18	1.5	2.5
19	1.0	1.6
20	1.0	1.9
21	1.2	2.2
22	0.9	1.6
23	2.9	4.7
24	1.4	2.9
25	1.6	2.7
26	0.8	1.3
27	2.1	3.4
28	0.5	1.1

Based on the results obtained from the corresponding clustering, it is then possible to define current thermal inertia classes, identifying to their response to short- (subscript S in the classes) and long- (subscript L in the classes) term, see Fig. 7. Boundary values to define the classes can be also evaluated, as seen in Table 9. These values are determined from the application of the proposed methodology for the specific case study. These limits can be considered as a first attempt to a classification approach, as they are only based on this case study. The greater the number of buildings to which the proposed methodology is applied, the greater the robustness of the clustering. It may also involve changing the numerical threshold values and class size to be defined. However, the purpose of this work is to describe and assess the methodology, evaluating its potential effectiveness and application for energy flexibility purposes based on dynamic thermal building clustering. With this aim, the corresponding dynamic behavior of buildings during DR events in varying inertia classes is discussed in detail in the next section.

4.1.2. Validation of the classification with the application of DR events: Evaluation and discussion

Two types of DR events are applied to validate the methodology: (i) a short-term and (ii) a long-term DR event. The first DR event consists of switching-off the cooling system for 5 min during the hour of peak demand (i.e., 1p.m.). On the other hand, the long-term DR event (ii) is achieved by switching off the cooling system for 2 h, starting at 1p.m. (i.e., the time when the peak occurs). The analysis is shown on a representative day (i.e., day with the outdoor temperature closest to the seasonal average). To evaluate the different response of the buildings, an approach similar to that proposed by Huang *et al.* [48] is adopted to differentiate the thermal inertia level of the buildings in different classes. Indeed, Huang *et al.* suggested considering the speed of zone temperature change in response to the DR event. In particular, the increase in indoor air temperature at the end of the event (ΔT_i) is determined, i.

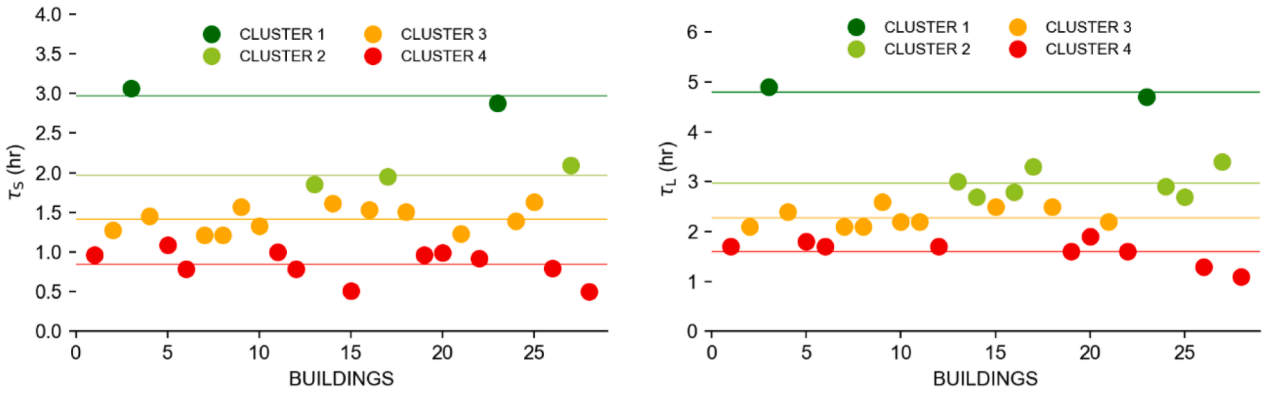

Fig. 6. Clustering results from the case study (the straight line represents the centroid for each cluster). (a) clustering based on short-term and (b) long-term response.

Table 7
Buildings in each cluster (short-term response).

Cluster	Buildings
1	3, 23
2	13, 17, 27
3	2, 4, 7, 8, 9,10, 14, 16, 18, 21,24,25
4	1, 5, 6, 11,12, 15,19, 20, 22, 26, 28

Table 8
Buildings in each cluster (long -term response).

Cluster	Buildings
1	3, 23
2	13, 14, 16, 17, 24, 25, 27
3	2, 4, 7, 8, 9, 10, 11, 15, 18, 21
4	1, 5, 6, 12, 19, 20, 22, 26, 28

e., after 5 min in the case of the short event and after 2 h in the case of the long event. Results are shown in Figures 8 and 9 by grouping buildings according to the corresponding thermal inertia classes (i.e., according to clustering, see Table 9). Fig. 8 shows ΔT_i values, including both the short-term (Fig. 8a) and long-term (Fig. 8b) classification for short and long-term DR events respectively. In Fig. 9, the averaged internal temperature variation is calculated by current thermal inertia class and type of event: short term DR event in Fig. 9a and long-term DR event in Fig. 9b. Note how the design classification is effective in distinguishing the dynamic behavior of buildings during DR events. In fact, passing from class A (high performance) to class D (low performance), both for short- and long-lasting DR events, ΔT_i decreases. Indeed, it is deduced that the internal air temperature evolution during the short-term DR event increases by 0.8 %, 1.2 %, 1.7 % and 2.6 % respectively for classes A_S, B_S, C_S and D_S. Regarding the values for long-term DR events, the increasing percentages of the average temperature are 12.6 %, 17.9 %, 19.1 %, 22.2 % respectively for classes A_L, B_L, C_L and D_L. This key finding of this paper is that the temperature variation indeed correlates with the clusters. Therefore, the clusters can be used to anticipate the effect that the DR events will have on the buildings, and subsequently to define ad hoc events for each cluster.

Fig. 10 shows the dynamic behavior, in terms of indoor air temperature, of a representative building (i.e., ID 3, 13,7,6) for each class during a short-term (Fig. 10a) and a long-term (Fig. 10b) DR event. This evolution also demonstrates the suitability of building labeling. In fact, for both types of events, the speed of the internal air temperature T_i increases, with the cooling system off, increases from class A (high performance) to class D (low performance).

Fig. 11 shows the labeling of buildings according to the flexibility

Table 9
Thermal inertia classes limit values.

CLASS	Short term (subscript S)	Long term (subscript L)
A	$\tau_S \geq 2.9$ hr	$\tau_L \geq 4.7$ hr
B	$1.6 < \tau_S < 2.9$ hr	$2.7 \leq \tau_L < 4.7$
C	$1.1 < \tau_S \leq 1.6$ hr	$1.9 < \tau_L < 2.7$
D	$\tau_S \leq 1.1$ hr	$\tau_L \leq 1.9$ hr

Fig. 7. Classes of thermal inertia identified with respect to values of time constants: (a) τ_S and (b) τ_L.

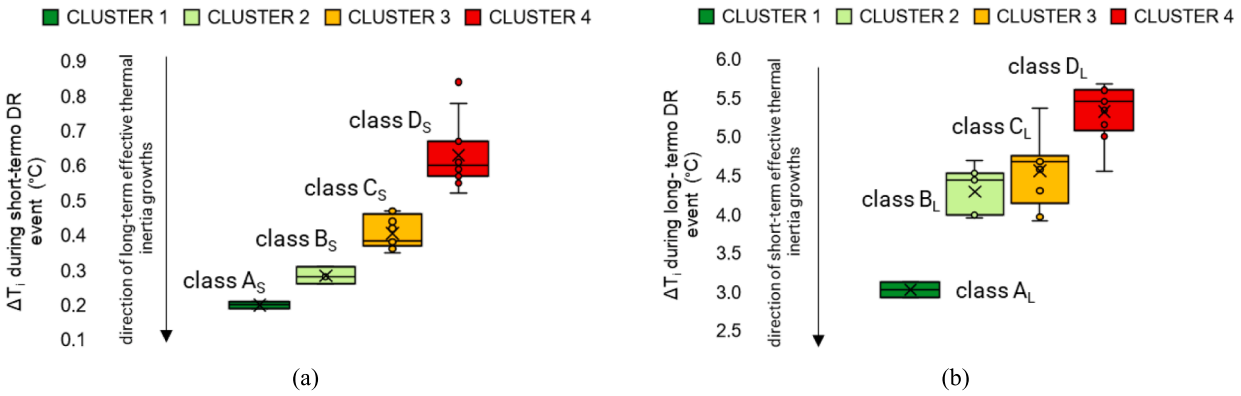

Fig. 8. Increase in indoor air temperature during ideal DR events for all case study buildings grouped by cluster: (a) short-term DR and (b) long-term DR event.

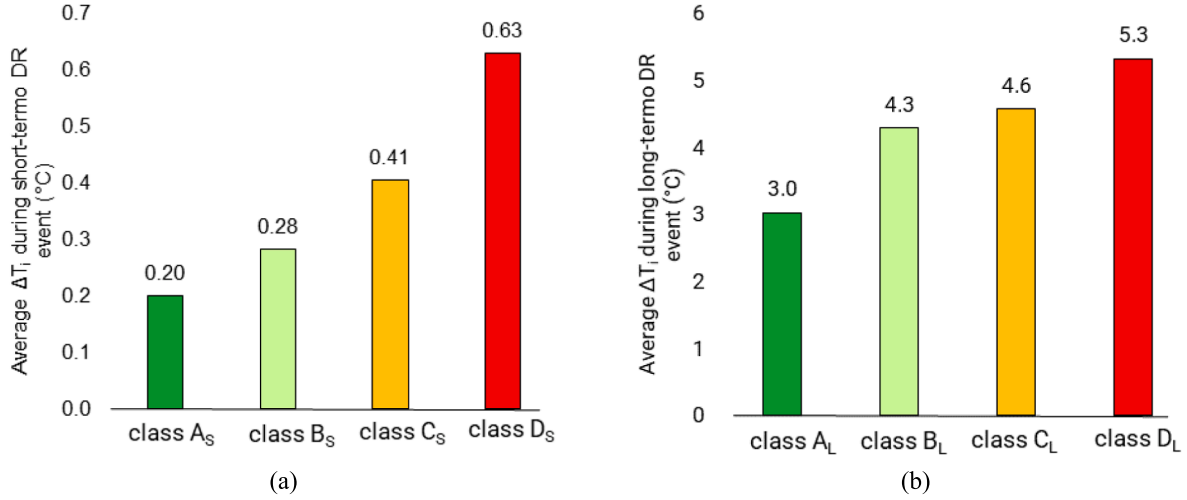

Fig. 9. Average increase in indoor air temperature for each class (obtained as the arithmetic mean of the results in Figure 8: (a) short-term and (b) long-term DR event.

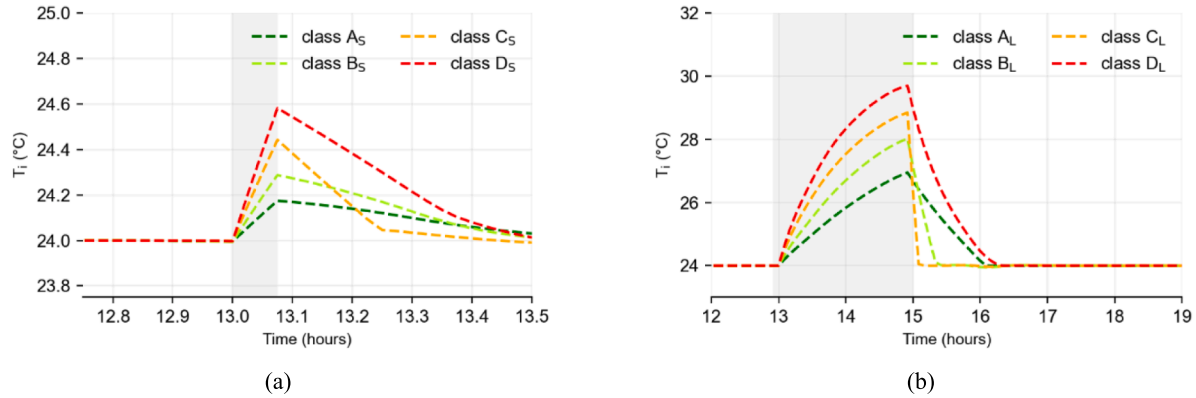

Fig. 10. Focus on the internal node temperature during a DR event for a representative building in each cluster: (a) short-term and (b) long-term DR event.

classes, summarizing the main results of the design characterization; Fig. 11a for short term and Fig. 11b for long term DR events. Moreover, Fig. 11 depicts the results distinguishing the construction periods of the buildings. As can be seen, it is not possible to deduce a classification of current thermal inertia available exclusively based on the knowledge of the design thermal and geometric characteristics (i.e., design thermal losses and floor area) of the corresponding building. In fact, a direct dependence between the year of construction and the thermal inertia class cannot be deduced. Fig. 12 shows the distribution of the values of the time constants (both short- and long-term) in relation to the construction age. As can be seen, no dependency can be observed.

The same conclusion can be affirmed if thermal (Figs. 13a) and geometric (Figs. 13b) characteristics are considered. These results confirm the extremely dynamic nature of energy flexibility as a

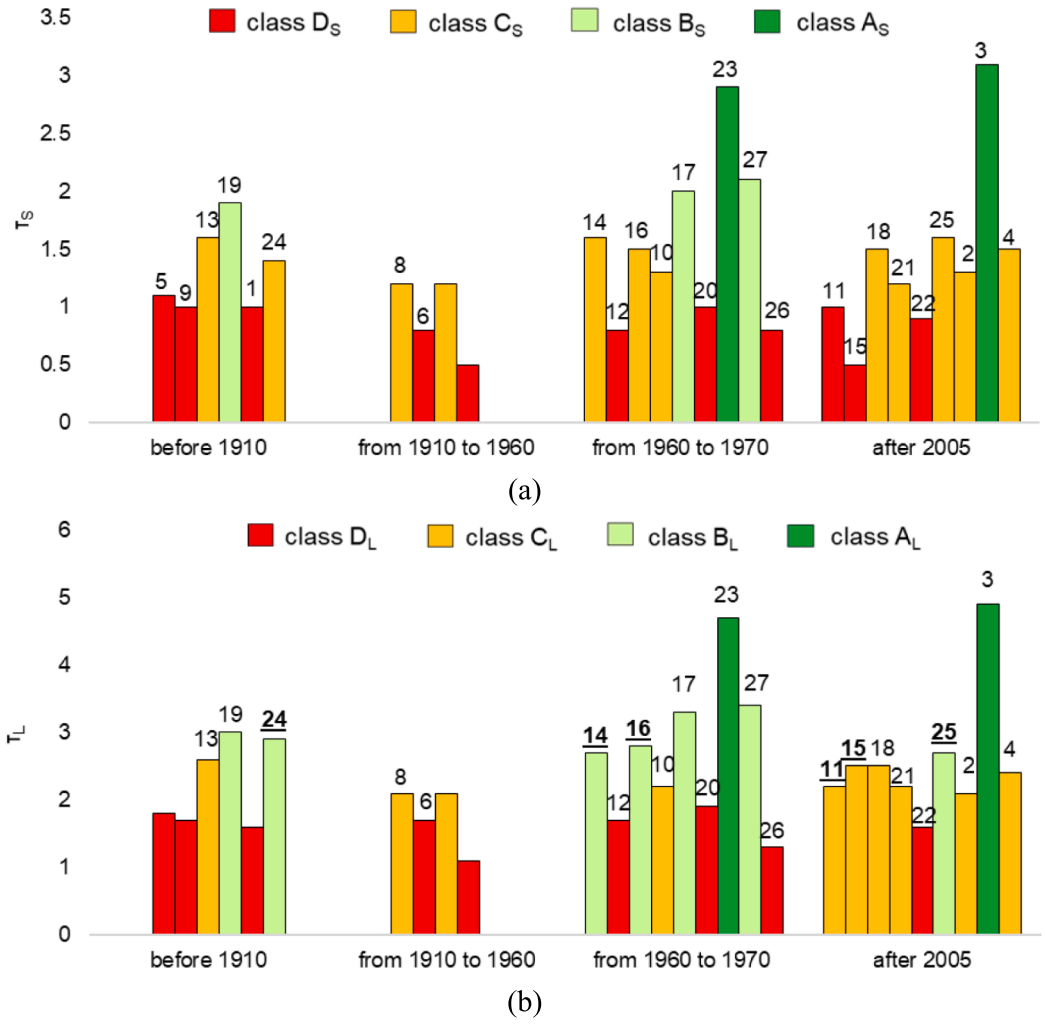

Fig. 11. Comparison between short and long-term inertia classes for each building (buildings changing class are in bold):(a) short-term and (b) long-term DR event.

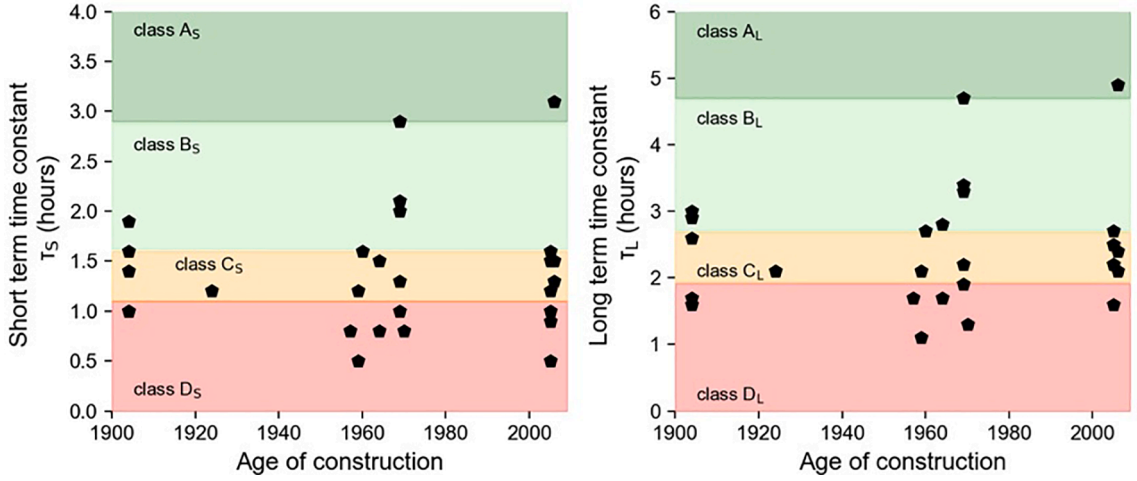

Fig. 12. Distribution of the values of the time constants calculated for the case study as a function of construction epoch.

characteristic of the building, reinforcing the need to provide dynamic models for a proper quantification.

Furthermore, also a T-test for independent samples has been used to verify the independence between the year of construction between clusters. This test is a robust and widely recognized statistical tool in scientific research. This is particularly suitable for comparing the means of two groups when the samples are independent, and the data are normally distributed. In the context of our study, the T-test has been used to evaluate whether it is significant to differentiate clusters by the construction year. By applying the T-test, the authors evaluate if a

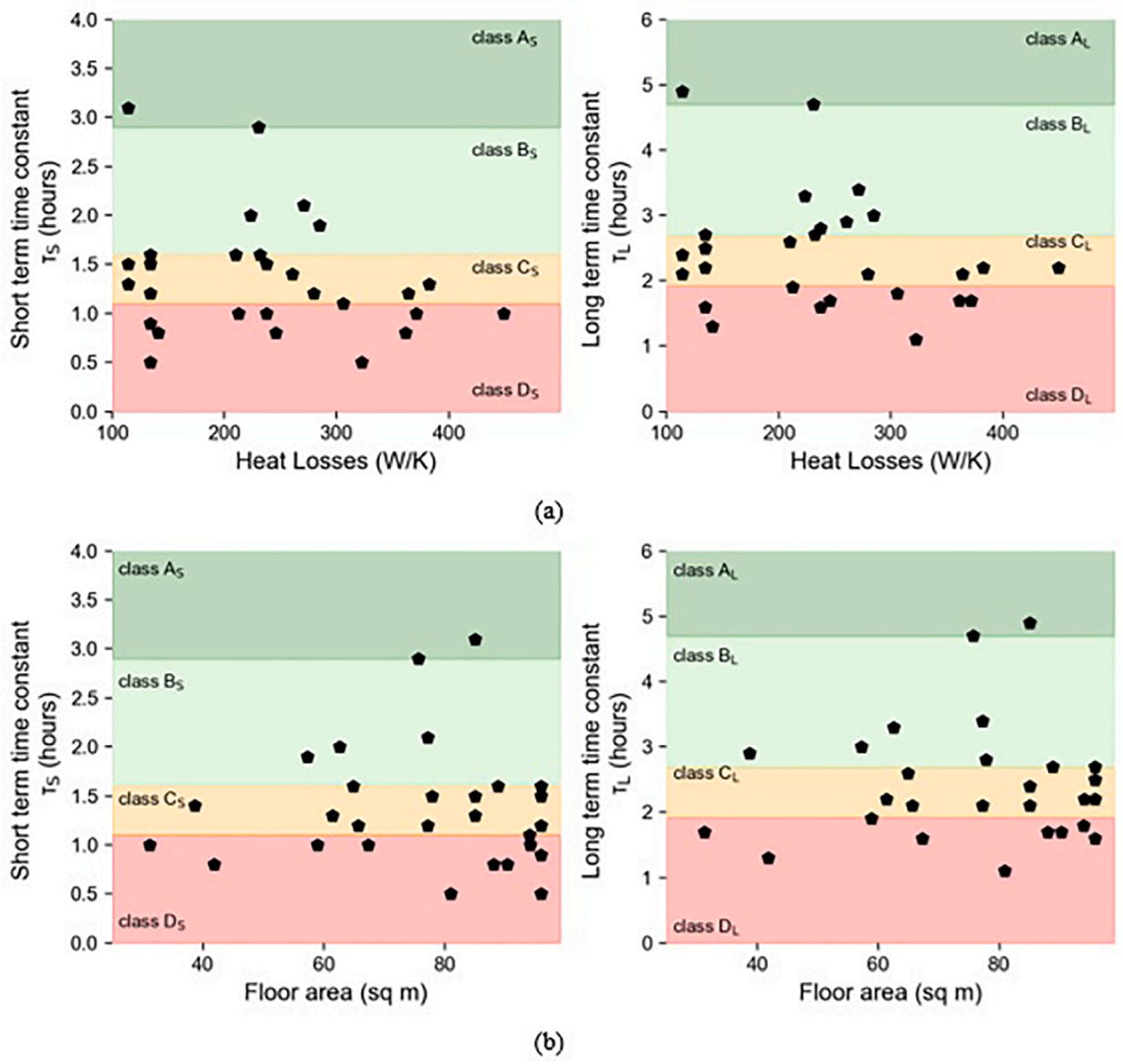

Fig. 13. Distribution of the values of the time constants calculated for the case study as a function of (a) thermal (i.e., heat losses) and (b) geometrical properties (i.e., floor area).

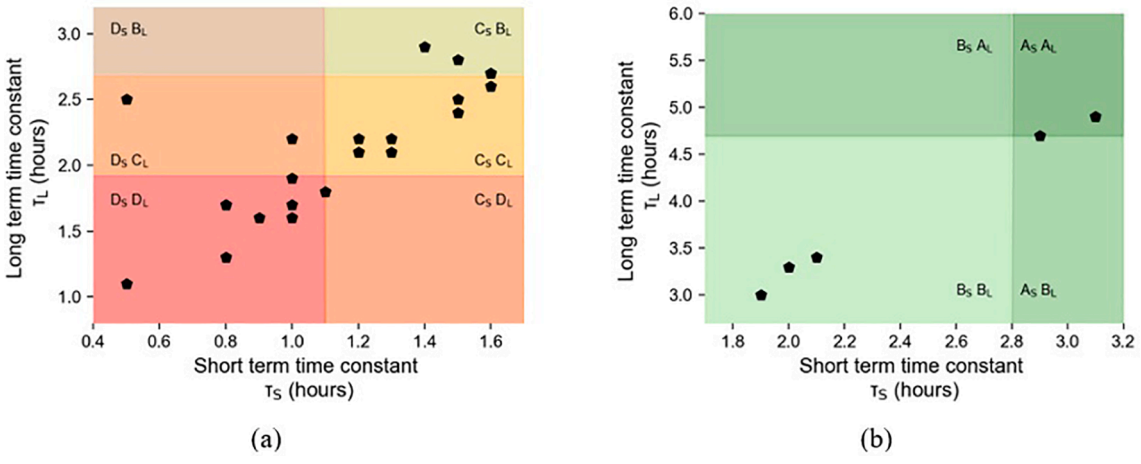

Fig. 14. Distribution of the values of the long-term time constant calculated for the case study as a function of the values of the short-term time constant: (a) focus on low classes and (b) focus on high classes.

simple classification by age is more adequate than the cluster. In all comparative cases between two samples: cluster 1 and 2, cluster 1 and 3, and cluster 1 and 4, p-values were greater than 0.05. These results indicate that the absence of statistically significant differences in the average construction years among the examined clusters suggests that the year of construction, as a variable, is not a factor to effectively differentiate among the different clusters. Therefore, it can be concluded that the year of construction does not provide an effective distinguishing criterion among the existing clusters.

Fig. 11 also gives additional information to distinguish buildings for which a change in the whole class is observed when assessing the short- and long-term response capacity. These buildings (buildings ID 11, 14, 15, 16, 24 and 25) represent approximately 21 % of the observed sample. Given the limited number of case studies analyzed, this percentage cannot be overlooked. Fig. 14 shows the values of the short-term and long-term time constants calculated for the case study buildings; distinguishing buildings classified in low inertia classes (Fig. 14a) from those in higher classes (Fig. 14b). Since the values of the time constants are obtained from analytical calculations, the observation of Fig. 14a, which contains the greatest number of data, combined with the non-negligible percentage of buildings with changing inertia classes, allows to confirm the need to distinguish the classification according to the duration of involvement in a DR event. In contrast, Fig. 14b seems to suggest a linear dependence between the values of the short-term and long-term time constants. However, given the small number of samples in this area, this behavior cannot be confirmed. Further buildings should be tested to confirm what was preliminarily observed.

With this aim, Fig. 15 proposes a focus on the dynamic behavior of two buildings: ID 9 and ID 15. Regarding building ID 9, there is no class change from short-term to long-term characterization (class C_L/C_S). However, building ID 15 presents a class change from class C_L to D_S. After the long DR event; i.e., after 2 h highlighted with the grey area in Fig. 15, both two buildings achieve approximately the same internal temperature increasing (i.e., 4.66 °C for building ID 9 and 4.74 °C for building ID 15). Note that, instead the dynamic evolution of the temperatures of the two buildings for a shorter time than the start time of the event, building ID 15 (class D_S) increases its internal temperature faster than building ID 9 (class C_S). For example, 5-minute time interval after the starting of the DR event, the difference between both temperatures is about 0.42 °C. This difference reaches its maximum value 15 min after the starting of the DR event, red area in Fig. 15, where the difference between the two temperatures is 0.63 °C.

4.2. Operative characterization

Regarding the numerical values of the solar irradiation defined in Table 5, the result of the operative characterization is discussed in this section. As was previously described in Sections 2 and 3, it is necessary to specify the season of the analysis. Subsequently, the results are then separated according to heating or cooling demand requirements. With this aim, Figures 16 and 176 show the percentual variation of the corresponding time constants (for short term in Fig. 16 and long-term DR events in Fig. 17 respectively) with respect to the design characterization (see Table 6 as well as the season (i.e., heating and cooling demand) and climate zone change (see Table 5). From these results, the numerical value of the time constants increases for each building considering the effect of internal gains for heating seasons. This pattern remains consistent for both time constants: τ_S (Fig. 16a) and τ_L (Fig. 17a). Moreover, the percentage increase tends to increase from climatic zone 1 (cold climate without dry season and with cold summer) to 6 (temperate climate with dry and hot summer). An inverse dependency is observed for the case of the cooling season, given in Fig. 16b and 17b. In this case, in fact, the numerical value of the time constants in the operative characterization remains lower than or equal to that obtained with the design characterization. Reduction percentages here also tend to increase from climate zone 1 to climate zone 6 with 33 % reduction for τ_S (Fig. 16b) and 68 % reduction for τ_L (Fig. 17b).

With regard to the thresholds identified for the classes, see Table 9, such changes in the value of the time constants can lead to a change in class for the same building as the operating conditions change. Further information can be found in Annex B, where extensive results corresponding to the operative characterization are given in detail. Class changes are highlighted in bold. Note that the greater the thermal gains, the more the building can aspire to high performance thermal inertia classes (i.e., going from D to A) for the heating season. This trend reverses for the cooling season: as the heat gains increases, the labeling of the building moves towards lower performance classes (i.e., going from A to D). However, this fact does not apply to all buildings, though it is also an intrinsic characteristic of the building that only emerges after applying the characterization methodology.

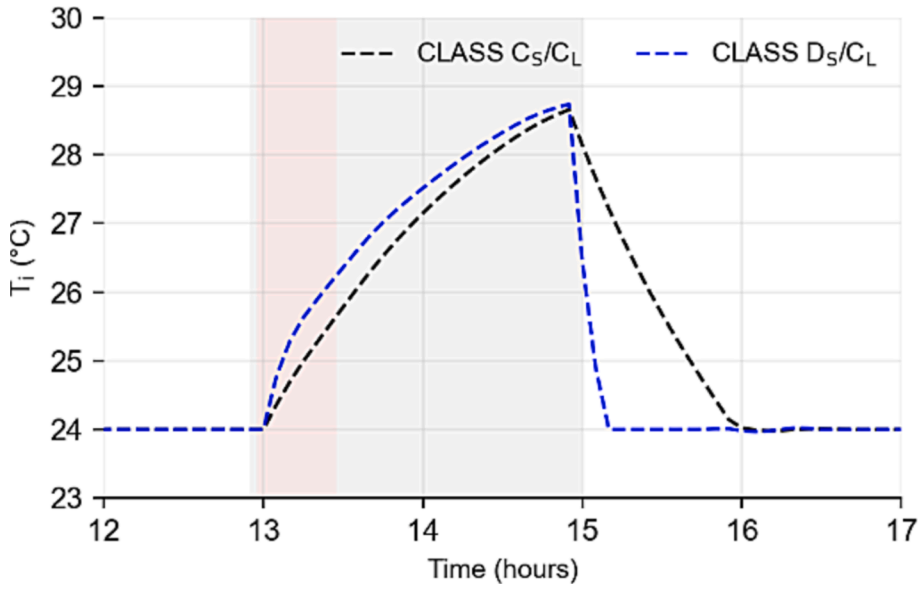

Fig. 15. Comparison during a long-term DR event between a building that does not change class (building 9 class C_L/C_S) a building that changes class (building 15 D_S/C_S).

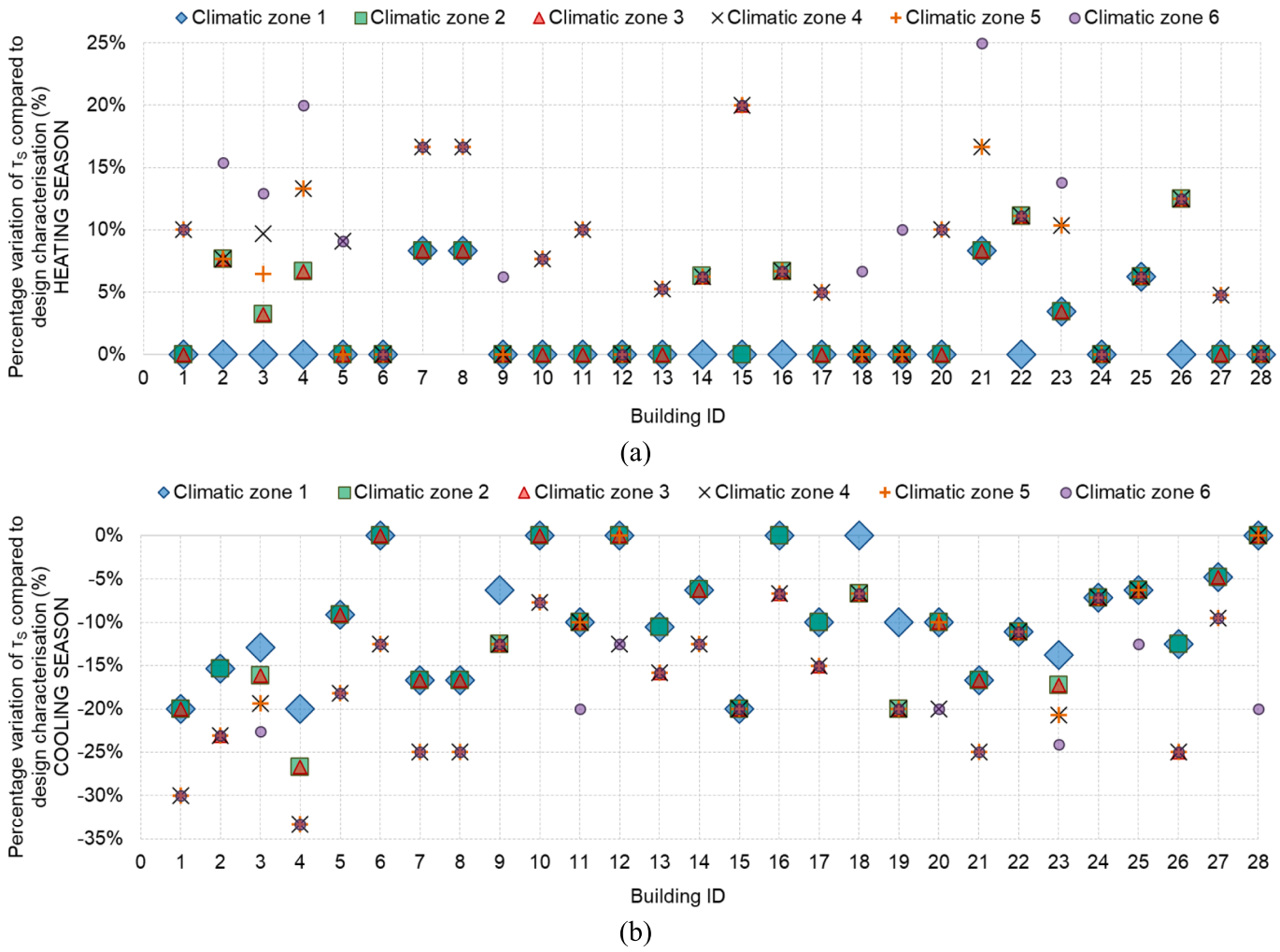

Fig. 16. Percentage variation of τ_S compared to design characterization as the climatic zone varies: (a) heating season and (b) cooling season.

4.3. *Discussion: How the method could be used by a DR agent?*

The application of the methodology to the case study remarked the relevance of both distinctions introduced for the characterization of the building during DR events (i.e., characterization according to the observed duration of the response and according to the design or operational level). Design characterization has proven essential for classifying buildings exclusively based on their intrinsic design features. (e.g., construction materials, size, type of fixtures). On the other hand, the application of the same proposed methodology considering the boundary conditions (typical of the particular application) points out the dynamic response variations of the building, only depending on the corresponding operation.

In light of these results, the proposed methodology is able to be applied in the following way by a DR agent, who can involve a portfolio of buildings such as those in the case study. Firstly, the agent should apply the design characterization to define the limits of the short-term and long-term inertia classes, either with a data-driven method or by direct characterization. The agent can already have an overview of the characteristics of the individual buildings available. Subsequently, based on the actual operational boundary conditions and grid requirements, the agent can apply operational characterization to plan involvement scenarios. In addition, the proposed methodology is adaptable for cluster-level demand response events by merely adjusting the boundary conditions and reevaluating the time constants.

The methodology straightforward application and the transparency of its performance indicators affirm its suitability for validation under design and highly operational scenarios. In this method, the lack of information relating to power and/or shiftable energy could be a possible drawback. However, the authors are confident that the arrival of more connected devices under the IoT paradigm will bridge this issue and not represent a barrier to the proposed methodology. What is more, the proposed methodology does not allow for a direct assessment of the building recovery phase to undisturbed conditions (i.e., before the DR event). In this phase, in fact, undesirable effects could be observed in the demand curve of the building, due to delayed power peaks to restore the building to its pre-event condition. However, it should be emphasized that the proposed methodology is based on the analytical characterization of the thermal mass of buildings. Thus, the different aspects considered in the characterization (e.g. the heating and cooling system) depend on the data used to identify the LPM. All the way these aspects should be also considered in the operational planning of building involvement. Note that the proposed methodology estimates the thermal response of the building also considering the thermal discomfort caused to customers (i.e., evaluated as the variation in the internal air temperature compared to comfort set-point). Additional proposals of quantifying displaced power/energy could be related to the proposed methodology to complete the global overall view of a DR agent in a multidimensional approach.

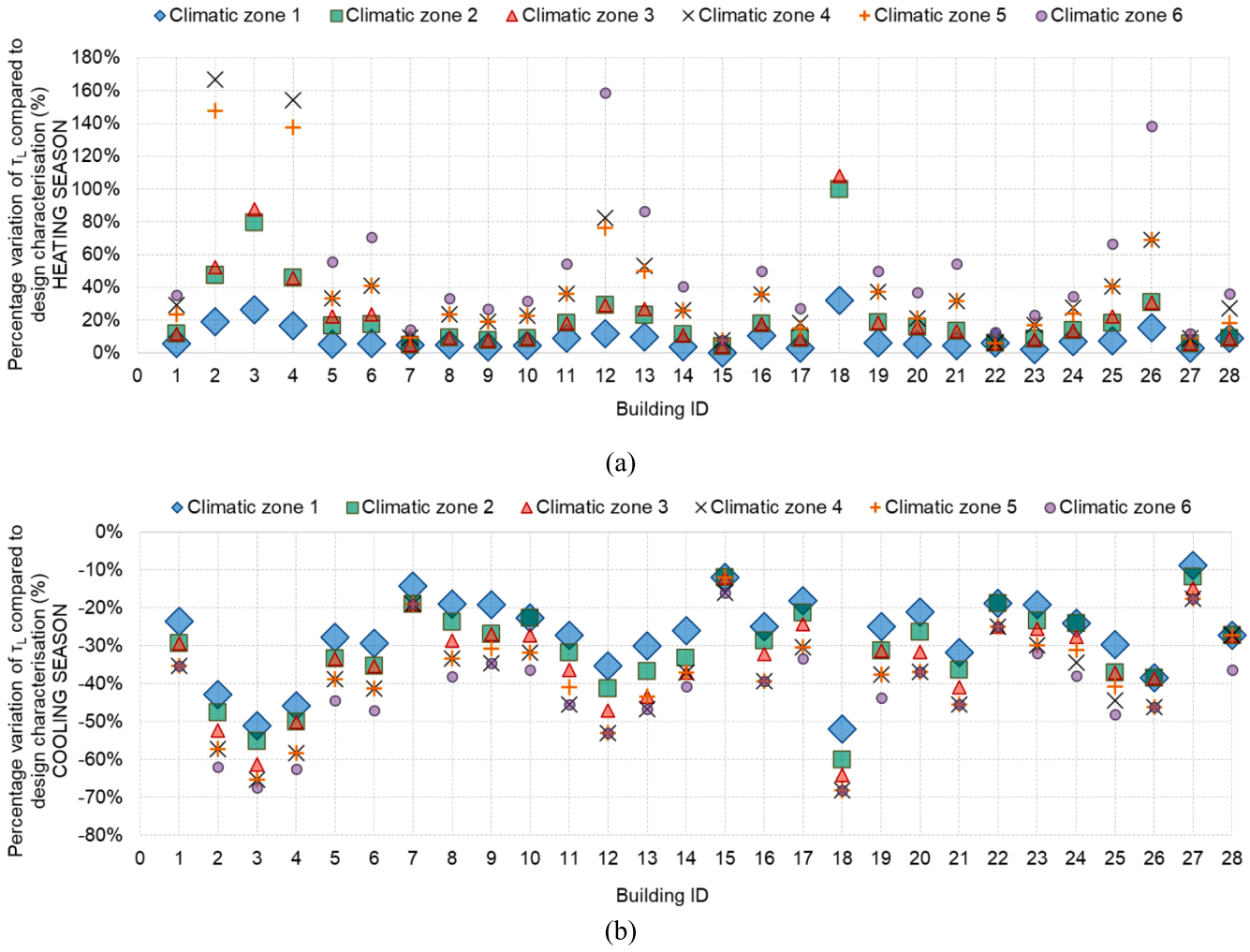

Fig. 17. Percentage variation of τ_L compared to design characterization as the climatic zone varies: (a) heating season and (b) cooling season.

5. Conclusions

This paper describes an innovative methodology to characterize the dynamic thermal response of building under demand response events. The proposed methodology complements the conventional approach for quantifying building energy flexibility. In fact, it allows to quantify the thermal mass to be exploited in buildings under DR events and depending on each event duration. The methodology allows the analytical characterization of the dynamic behavior of buildings, regardless of the type of demand response event and specific boundary conditions (such as weather or season). Actually, and due to this dynamic nature of the building energy flexibility characterization, the proposed methodology requires the definition of a lumped parameter model for each building. The model can be then defined both in the presence of measured data and only based on the design characteristics of the building. Simulations allow to calculate two indicators: the characteristic time constants of the building. These time constants quantify the ability of the building to respond under DR events both short-term and long-term conditions. Based on the values of such time constants, classes of thermal inertia can be defined. Two different characterization objectives are introduced: (i) design characterization, buildings are labeled only based on their intrinsic characteristics of the building themself (i.e., regardless of specific boundary conditions); and (ii) operative characterization, the time constants allow to consider the variability of the boundary conditions. To test the suitability of the proposed methodology, it is applied to a portfolio of 28 real residential buildings. The buildings differ in type, construction period and size. The main results obtained can be summarized in the following points.

- The methodology applied to the case study proved to be effective in distinguishing the different dynamic response capabilities of buildings during different demand response events.
- The subdivision into thermal inertia classes is representative of the different levels of thermal mass currently available in each building. It is also demonstrated by applying realistic demand response events to buildings labeled in different classes.
- It is essential to distinguish the duration of the event in the characterization. Some buildings showed a class change from short-term to long-term classification.
- It was found that it is not possible to deduce the dynamic response of a building in different demand response events only from its design characteristics.
- The introduction of the variability of the boundary conditions can lead to a different dynamic characterization of the building compared to the design one. However, it is also a characteristic that can only be evaluated after applying both the design and operational characterization methodology.

In conclusion, the study highlighted the dynamic nature of the energy flexibility of buildings and the need to introduce a characterization methodology that also includes the type of demand response event, not only the thermal building characteristics. The proposed methodology is

designed to be easily applicable, customizable and with results that are simple to interpret by a demand response agent. Note that this proposal is a preliminary application of the methodology. In fact, the inertia classes are obtained with reference only to the portfolio case study. In fact, the study can be considered as a starting point for the analytical characterization of buildings in a specific portfolio to be used by DR operators. However, even considering a reduced number of buildings, the time constants provided effective labeling of the buildings, allowing to facilitate the planning of building involvement scenarios based on different specific operating conditions.

CRediT authorship contribution statement

Alice Mugnini: Writing – review & editing, Writing – original draft, Validation, Software, Methodology, Conceptualization. **Alfonso P. Ramallo-González:** Writing – review & editing, Visualization, Supervision, Resources, Methodology, Data curation, Conceptualization. **Adelaida Parreño:** Writing – review & editing, Validation. **Angel Molina-Garcia:** Writing – review & editing, Visualization, Supervision, Conceptualization. **Antonio F. Skarmeta:** Supervision. **Alessia Arteconi:** Writing – review & editing, Supervision, Resources.

Declaration of competing interest

The authors declare that they have no known competing financial interests or personal relationships that could have appeared to influence the work reported in this paper.

Data availability

Data will be made available on request.

Acknowledgements

This project has been partly funded by project PHOENIX, Grant Agreement Number 893079.

This project has received funding from the European Union's Horizon 2020 research and innovation program under the Marie Skłodowska-Curie grant agreement No. 101007820. This publication reflects only the author's view, and the REA is not responsible for any use that may be made of the information it contains.

Appendix

Lumped parameter models to represent the dynamics of buildings. and characteristic of the case study.

Fig. A1. Percentage absolute values of LPM model fitting errors for each building in the case study.

Table A2
Main thermal and geometrical characteristics of the case study from the clipboard based assessment of the CHP Acceleration project from which the data of this study has been extracted [43].

ID	Floor area (sqm)	Type of building	Year	Wall area (sq m)	Wall U-Value (W sqm−1 K−1)	Glass area (sq m)	Glass type	Heat losses (W/K)
1	31.2	3rd floor of Mid Terrace	1904	67.84	3.26	7.7	Single	370.95
2	85	Mid Terrace	2006	57.77	0.2	19.7	Double	113.99
3	85	Mid Terrace	2006	57.77	0.2	19.7	Double	113.99
4	85	Mid Terrace	2006	57.77	0.2	19.7	Double	113.99
5	93.91	Detached Cottage	1790	107.67	0.9	22.81	Some Single, Some Double	305.43
6	90.26	Semi Detached	1957	71.56	2.12	25.69	missing	361.2
7	77.17	End Terrace	1959	97.6	0.76	17.9	Double	279.57
8	65.62	Semi Detached	1924	missing	missing	10.35	missing	363.74
9	64.86	3rd floor of Mid Terrace	1904	missing	missing	9.98	missing	209.67
10	61.33	Semi Detached	1969	73.68	missing	4.32	missing	382.33
11	94.06	Semi Detached	2005	missing	missing	20.14	missing	449.1
12	88	End Terrace	1964	88.46	1.63	14.07	missing	245.62
13	57.22	Mid Terrace	1904	missing	missing	5.04	missing	284.38
14	88.8	End Terrace	1960	89.87	0.62	13.5	missing	231.9
15	95.81	End Terrace	2005	78.68	0.63	11.94	mix of solid, triple and double	134.19
16	77.8	Semi Detached	1964	108	0.46	18.2	Double	237.19
17	62.52	End Terrace	1969	96.5	0.46	13.3	Single	223.33
18	95.81	Mid Terrace	2005	78.68	0.63	11.94	mix of solid, triple and double	134.19
19	67.27	3rd floor of Mid Terrace	1904	missing	2.2	7.19	missing	237.14
20	58.85	Mid Terrace	1969	86.2	0.76	13.5	Double	212.33
21	95.81	End Terrace	2005	78.68	0.63	11.94	Mix of solid, triple and double	134.19
22	95.81	End Terrace	2005	78.68	0.63	11.94	Mix of Solid, Triple and double	134.19
23	75.63	Terrace	1969	97.8	0.46	14.2	Double	230.62
24	38.66	Mid Terrace	1904	missing	1.2	8.52	missing	260.38
25	95.81	End Terrace	2005	78.68	0.63	11.94	mix of solid, triple and double	134.19
26	41.8	Semi Detached	1970	25.65	0.52	14.01	Double	140.69
27	77.17	Mid Terrace	1969	97.6	0.76	17.9	Double	270.71
28	80.9	End Terrace	1959	119.6	0.76	15.2	Single	322.1

Table A3
Numerical values of the LPMs [43].

ID	$1/R_1$ (W/K)	C_1 (Wh/K)	$1/R_2$ (W/K)	C_2 (Wh/K)	$1/R_3$ (W/K)	C_3 (Wh/K)	$1/R_4$ (W/K)	f_S (-)
1	191.06	91.13	84.7	143.09	84.18	4982.82	35.48	1.10
2	128.95	0.01	69.35	199.65	100.46	5135.95	53.53	3.05
3	166.88	62.44	0	573.49	162.49	4945.2	118.3	4.90
4	877.24	143.03	0	153.2	98.57	4866.32	66.74	2.03

(*continued on next page*)

Table A3 (*continued*)

ID	$1/R_1$ (W/K)	C_1 (Wh/K)	$1/R_2$ (W/K)	C_2 (Wh/K)	$1/R_3$ (W/K)	C_3 (Wh/K)	$1/R_4$ (W/K)	f_S (-)
5	252.92	1.12	174.48	322.52	141.92	4919.55	84.1	2.71
6	352.51	3002.51	368.61	734.79	275.16	5169.91	412.54	7.35
7	200.21	121.58	78.74	174.16	93.64	4992.06	34.11	0.49
8	200.14	120.89	78.81	174.12	93.9	4992.16	33.96	0.95
9	389.02	0.01	236.9	591.17	214.34	5204.82	90.71	2.28
10	609.32	0.18	380.08	844.13	563.41	4996.06	167.99	4.24
11	146.85	284.72	234.53	273.74	103.54	4947.87	82.43	2.31
12	355.74	3005.74	371.84	746.72	278.39	5173.14	420.02	10.58
13	451.05	286.63	0	495.8	199.7	5039.17	169.35	3.12
14	390.77	0	148.7	590.5	223.15	5179.46	123.56	2.94
15	0	131.24	332.01	65.45	68.45	1200.95	81.12	0.25
16	500.28	1000.28	366.38	1000.28	272.93	5167.68	201.39	5.12
17	255.71	2117.15	56.98	613.05	104.93	5294.83	151.89	1.65
18	514.57	314.57	214.57	1014.57	614.57	50,014.57	272.83	19.40
19	566.67	47.3	157.61	203.25	116.12	4493.08	10.42	1.87
20	268.2	314.9	180.29	266.49	105.15	5149.23	62.09	1.73
21	200.05	121.05	78.05	174.05	93.05	4992.05	33.27	1.35
22	263.84	93.83	109.46	242.55	172.33	4945.35	89.21	1.00
23	320.01	0.17	167.93	501.68	131.53	4921.23	0	0.96
24	158.26	1593.63	247.37	900.8	236.58	5253.78	311.42	3.38
25	413.89	0	277.8	631.6	233.23	5056.88	77.96	4.00
26	461.74	454.55	0.04	112.78	104.64	4896.19	89.2	1.95
27	452.64	0	156.79	1165.88	320.91	5016.19	234.87	1.41
28	976.77	3158.21	342.28	205.38	378.36	2774.62	4.76	2.26

ANNEX b

Results of the operative characterization

Table B1
Values of τ_S for different climatic zones (contribution of solar gains).

	Climatic zone											
	1		2		3		4		5		6	
ID	*winter*	*summer*	*winter*	*summer*	*winter*	*summer*	*winter*	*summer*	*winter*	*summer*	*winter*	*summer*
1	1.0	0.8	1.0	0.8	1.0	0.8	1.1	0.7	1.1	0.7	1.1	0.7
2	1.3	1.1	1.4	1.1	1.4	1.0	1.4	1.0	1.4	1.0	1.5	1.0
3	3.1	2.7	3.2	2.6	3.2	2.6	3.4	2.5	3.3	2.5	3.5	2.4
4	1.5	1.2	1.6	1.1	1.6	1.1	1.7	1.0	1.7	1.0	1.8	1.0
5	1.1	1.0	1.1	1.0	1.1	1.0	1.2	0.9	1.1	0.9	1.2	0.9
6	0.8	0.8	0.8	0.8	0.8	0.8	0.8	0.7	0.8	0.7	0.8	0.7
7	1.3	1.0	1.3	1.0	1.3	1.0	1.4	0.9	1.4	0.9	1.4	0.9
8	1.3	1.0	1.3	1.0	1.3	1.0	1.4	0.9	1.4	0.9	1.4	0.9
9	1.6	1.5	1.6	1.4	1.6	1.4	1.6	1.4	1.6	1.4	1.7	1.4
10	1.3	1.3	1.3	1.3	1.3	1.3	1.4	1.2	1.4	1.2	1.4	1.2
11	1.0	0.9	1.0	0.9	1.0	0.9	1.1	0.9	1.1	0.9	1.1	0.8
12	0.8	0.8	0.8	0.8	0.8	0.8	0.8	0.7	0.8	0.8	0.8	0.7
13	1.9	1.7	1.9	1.7	1.9	1.6	2.0	1.6	2.0	1.6	2.0	1.6
14	1.6	1.5	1.7	1.5	1.7	1.5	1.7	1.4	1.7	1.4	1.7	1.4
15	0.5	0.4	0.5	0.4	0.6	0.4	0.6	0.4	0.6	0.4	0.6	0.4
16	1.5	1.5	1.6	1.5	1.6	1.4	1.6	1.4	1.6	1.4	1.6	1.4
17	2.0	1.8	2.0	1.8	2.0	1.7	2.1	1.7	2.1	1.7	2.1	1.7
18	1.5	1.5	1.5	1.4	1.5	1.4	1.5	1.4	1.5	1.4	1.6	1.4
19	1.0	0.9	1.0	0.8	1.0	0.8	1.0	0.8	1.0	0.8	1.1	0.8
20	1.0	0.9	1.0	0.9	1.0	0.9	1.1	0.8	1.1	0.9	1.1	0.8
21	1.3	1.0	1.3	1.0	1.3	1.0	1.4	0.9	1.4	0.9	1.5	0.9
22	0.9	0.8	1.0	0.8	1.0	0.8	1.0	0.8	1.0	0.8	1.0	0.8
23	3.0	2.5	3.0	2.4	3.0	2.4	3.2	2.3	3.2	2.3	3.3	2.2
24	1.4	1.3	1.4	1.3	1.4	1.3	1.4	1.3	1.4	1.3	1.4	1.3
25	1.7	1.5	1.7	1.5	1.7	1.5	1.7	1.5	1.7	1.5	1.7	1.4
26	0.8	0.7	0.9	0.7	0.9	0.6	0.9	0.6	0.9	0.6	0.9	0.6
27	2.1	2.0	2.1	2.0	2.1	2.0	2.2	1.9	2.2	1.9	2.2	1.9
28	0.5	0.5	0.5	0.5	0.5	0.5	0.5	0.5	0.5	0.5	0.5	0.4

Table B2
Values of τ_L for different climatic zones (contribution of solar gains).

	Climatic zone											
	1		2		3		4		5		6	
ID	*winter*	*summer*	*winter*	*summer*	*winter*	*summer*	*winter*	*summer*	*winter*	*summer*	*winter*	*summer*
1	1.8	1.3	1.9	1.2	1.9	1.2	2.2	1.1	2.1	1.1	2.3	1.1
2	2.5	1.2	3.1	1.1	3.2	1	5.6	0.9	5.2	0.9	∞	0.8
3	6.2	2.4	8.8	2.2	9.2	1.9	∞	1.7	∞	1.7	∞	1.6
4	2.8	1.3	3.5	1.2	3.5	1.2	6.1	1	5.7	1	∞	0.9
5	1.9	1.3	2.1	1.2	2.2	1.2	2.4	1.1	2.4	1.1	2.8	1
6	1.8	1.2	2	1.1	2.1	1.1	2.4	1	2.4	1	2.9	0.9
7	2.2	1.8	2.2	1.7	2.2	1.7	2.3	1.7	2.3	1.7	2.4	1.7
8	2.2	1.7	2.3	1.6	2.3	1.5	2.6	1.4	2.6	1.4	2.8	1.3
9	2.7	2.1	2.8	1.9	2.8	1.9	3.1	1.7	3.1	1.8	3.3	1.7
10	2.3	1.7	2.4	1.7	2.4	1.6	2.7	1.5	2.7	1.5	2.9	1.4
11	2.4	1.6	2.6	1.5	2.6	1.4	3	1.2	3	1.3	3.4	1.2
12	1.9	1.1	2.2	1	2.2	0.9	3.1	0.8	3	0.8	4.4	0.8
13	3.3	2.1	3.7	1.9	3.8	1.7	4.6	1.6	4.5	1.7	5.6	1.6
14	2.8	2	3	1.8	3	1.7	3.4	1.7	3.4	1.7	3.8	1.6
15	2.5	2.2	2.6	2.2	2.6	2.2	2.7	2.1	2.7	2.2	2.7	2.1
16	3.1	2.1	3.3	2	3.3	1.9	3.8	1.7	3.8	1.7	4.2	1.7
17	3.4	2.7	3.6	2.6	3.6	2.5	3.9	2.3	3.8	2.3	4.2	2.2
18	3.3	1.2	5	1	5.2	0.9	∞	0.8	∞	0.8	∞	0.8
19	1.7	1.2	1.9	1.1	1.9	1.1	2.2	1	2.2	1	2.4	0.9
20	2	1.5	2.2	1.4	2.2	1.3	2.3	1.2	2.3	1.2	2.6	1.2
21	2.3	1.5	2.5	1.4	2.5	1.3	2.9	1.2	2.9	1.2	3.4	1.2
22	1.7	1.3	1.7	1.3	1.7	1.2	1.7	1.2	1.7	1.2	1.8	1.2
23	4.8	3.8	5.1	3.6	5.1	3.5	5.5	3.3	5.5	3.3	5.8	3.2
24	3.1	2.2	3.3	2.2	3.3	2.1	3.7	1.9	3.6	2	3.9	1.8
25	2.9	1.9	3.2	1.7	3.3	1.7	3.8	1.5	3.8	1.6	4.5	1.4
26	1.5	0.8	1.7	0.8	1.7	0.8	2.2	0.7	2.2	0.7	3.1	0.7
27	3.5	3.1	3.6	3	3.6	2.9	3.7	2.8	3.7	2.8	3.8	2.8
28	1.2	0.8	1.2	0.8	1.2	0.8	1.4	0.8	1.3	0.8	1.5	0.7

Table B3
Short-term inertia classes for each building with the contribution of the solar gains.

		Climatic zone											
		1		2		3		4		5		6	
ID	Class*	*winter*	*summer*	*winter*	*summer*	*winter*	*summer*	*winter*	*summer*	*winter*	*summer*	*winter*	*summer*
1	**D_S**	C_S	D_S	D_S	D_S	D_S	D_S	D_S	D_S	D_S	D_S	C_S	D_S
2	**C_S**	C_S	C_S	C_S	D_S	C_S	D_S	C_S	D_S	C_S	D_S	C_S	D_S
3	**A_S**	A_S	B_S	A_S	B_S	A_S	B_S	A_S	B_S	A_S	B_S	A_S	B_S
4	**C_S**	C_S	C_S	C_S	C_S	C_S	D_S	B_S	D_S	B_S	D_S	B_S	D_S
5	**D_S**	C_S	D_S	C_S	D_S	C_S	D_S	C_S	D_S	C_S	D_S	C_S	D_S
6	**D_S**	D_S	D_S	D_S	D_S	D_S	D_S	D_S	D_S	D_S	D_S	D_S	D_S
7	**C_S**	C_S	D_S	C_S	D_S	C_S	D_S	C_S	D_S	C_S	D_S	C_S	D_S
8	**C_S**	C_S	D_S	C_S	D_S	C_S	D_S	C_S	D_S	C_S	D_S	C_S	D_S
9	**C_S**	C_S	C_S	C_S	C_S	C_S	C_S	B_S	C_S	B_S	C_S	B_S	C_S
10	**C_S**	C_S	C_S	C_S	C_S	C_S	C_S	C_S	C_S	C_S	C_S	C_S	C_S
11	**D_S**	D_S	D_S	D_S	D_S	D_S	D_S	D_S	D_S	D_S	D_S	D_S	D_S
12	**D_S**	D_S	D_S	D_S	D_S	D_S	D_S	D_S	D_S	D_S	D_S	D_S	D_S
13	**B_S**	B_S	B_S	B_S	B_S	B_S	B_S	B_S	C_S	B_S	C_S	B_S	C_S
14	**C_S**	B_S	C_S	B_S	C_S	B_S	C_S	B_S	C_S	B_S	C_S	B_S	C_S
15	**D_S**	D_S	D_S	D_S	D_S	D_S	D_S	D_S	D_S	D_S	D_S	D_S	D_S
16	**C_S**	C_S	C_S	C_S	C_S	C_S	C_S	C_S	C_S	C_S	C_S	C_S	C_S
17	**B_S**	B_S	B_S	B_S	B_S	B_S	B_S	B_S	B_S	B_S	B_S	B_S	B_S
18	**C_S**	C_S	C_S	C_S	C_S	C_S	C_S	C_S	C_S	C_S	C_S	C_S	C_S
19	**D_S**	D_S	D_S	D_S	D_S	D_S	D_S	D_S	D_S	D_S	D_S	D_S	D_S
20	**D_S**	D_S	D_S	D_S	D_S	D_S	D_S	D_S	D_S	D_S	D_S	D_S	D_S
21	**C_S**	C_S	D_S	C_S	D_S	C_S	D_S	C_S	D_S	C_S	D_S	C_S	D_S
22	**D_S**	D_S	D_S	D_S	D_S	D_S	D_S	D_S	D_S	D_S	D_S	D_S	D_S
23	**A_S**	A_S	B_S	A_S	B_S	A_S	B_S	A_S	B_S	A_S	B_S	A_S	B_S
24	**C_S**	C_S	C_S	C_S	C_S	C_S	C_S	C_S	C_S	C_S	C_S	C_S	C_S
25	**C_S**	B_S	C_S	B_S	C_S	B_S	C_S	B_S	C_S	B_S	C_S	B_S	C_S
26	**D_S**	D_S	D_S	D_S	D_S	D_S	D_S	D_S	D_S	D_S	D_S	D_S	D_S
27	**B_S**	B_S	B_S	B_S	B_S	B_S	B_S	B_S	B_S	B_S	B_S	B_S	B_S
28	**D_S**	D_S	D_S	D_S	D_S	D_S	D_S	D_S	D_S	D_S	D_S	D_S	D_S

* Short-term labeling with design characterization

Table B4
Long-term inertia classes for each building with the contribution of the solar gains.

		Climatic zone											
		1		2		3		4		5		6	
ID	Class*	*winter*	*summer*	*winter*	*summer*	*winter*	*summer*	*winter*	*summer*	*winter*	*summer*	*winter*	*summer*
1	**D_L**	D_L	D_L	D_L	D_L	D_L	D_L	C_L	D_L	C_L	D_L	C_L	D_L
2	**C_L**	C_L	D_L	BL	D_L	BL	D_L	A_L	D_L	A_L	D_L	A_L	D_L
3	**A_L**	A_L	C_L	A_L	C_L	A_L	D_L	A_L	D_L	A_L	D_L	A_L	D_L
4	**C_L**	BL	D_L	B_L	D_L	B_L	D_L	A_L	D_L	A_L	D_L	A_L	D_L
5	**D_L**	D_L	D_L	C_L	D_L	C_L	D_L	C_L	D_L	C_L	D_L	B_L	D_L
6	**D_L**	D_L	D_L	C_L	D_L	C_L	D_L	C_L	D_L	C_L	D_L	B_L	D_L
7	**C_L**	CL	D_L	C_L	D_L	C_L	D_L	C_L	D_L	C_L	D_L	C_L	D_L
8	**C_L**	CL	D_L	C_L	D_L	C_L	D_L	C_L	D_L	C_L	D_L	B_L	D_L
9	**C_L**	B_L	C_L	B_L	D_L	B_L	D_L	B_L	D_L	B_L	D_L	B_L	D_L
10	**C_L**	C_L	D_L	C_L	D_L	C_L	D_L	B_L	D_L	B_L	D_L	B_L	D_L
11	**C_L**	C_L	D_L	C_L	D_L	C_L	D_L	B_L	D_L	B_L	D_L	B_L	D_L
12	**D_L**	D_L	D_L	C_L	D_L	C_L	D_L	B_L	D_L	B_L	D_L	B_L	D_L
13	**B_L**	B_L	C_L	B_L	D_L	B_L	D_L	B_L	D_L	B_L	D_L	A_L	D_L
14	**B_L**	B_L	C_L	B_L	D_L	B_L	D_L	B_L	D_L	B_L	D_L	B_L	D_L
15	**C_L**	C_L	C_L	C_L	C_L	C_L	C_L	B_L	C_L	B_L	C_L	B_L	C_L
16	**B_L**	B_L	C_L	B_L	C_L	B_L	D_L	B_L	D_L	B_L	D_L	B_L	D_L
17	**B_L**	B_L	B_L	B_L	C_L	B_L	C_L	B_L	C_L	B_L	C_L	B_L	C_L
18	**C_L**	B_L	D_L	A_L	D_L	A_L	D_L	A_L	D_L	A_L	D_L	A_L	D_L
19	**D_L**	D_L	D_L	D_L	D_L	D_L	D_L	C_L	D_L	C_L	D_L	C_L	D_L
20	**D_L**	C_L	D_L	C_L	D_L	C_L	D_L	C_L	D_L	C_L	D_L	C_L	D_L
21	**C_L**	C_L	D_L	C_L	D_L	C_L	D_L	B_L	D_L	B_L	D_L	B_L	D_L
22	**D_L**	D_L	D_L	D_L	D_L	D_L	D_L	D_L	D_L	D_L	D_L	D_L	D_L
23	**A_L**	A_L	B_L	A_L	B_L	A_L	B_L	A_L	B_L	A_L	B_L	A_L	B_L
24	**B_L**	B_L	C_L	B_L	C_L	B_L	C_L	B_L	D_L	B_L	C_L	B_L	D_L
25	**B_L**	B_L	D_L	B_L	D_L	B_L	D_L	B_L	D_L	B_L	D_L	B_L	D_L
26	**D_L**	D_L	D_L	D_L	D_L	D_L	D_L	C_L	D_L	C_L	D_L	B_L	D_L
27	**B_L**	B_L	B_L	B_L	B_L	B_L	B_L	B_L	B_L	B_L	B_L	B_L	B_L
28	**D_L**	D_L	D_L	D_L	D_L	D_L	D_L	D_L	D_L	D_L	D_L	D_L	D_L

* Long-term labeling with design characterization

References

[1] European Commission. The European Green Deal. 2019. Available on-line: https://eur-lex.europa.eu/legal-content/EN/TXT/?uri=COM%3A2019%3A640%3AFIN (access verified on 11/09/2023)..

[2] International Energy Agency. Net Zero Emissions by 2050 Scenario (NZE). 2023. Available on-line: www.iea.org/reports/global-energy-and-climate-model/net-zero-emissions-by-2050-scenario-nze (access verified on 13/09/2023).

[3] International Energy Agency. Renewable Energy Policies in a Time of Transition: Heating and Cooling. 2020. Available on-line www.iea.org/reports/renewable-energy-policies-in-a-time-of-transition-heating-and-cooling (access verified on 11/09/2023).

[4] International Energy Agency. Energy security Reliable, affordable access to all fuels and energy sources). 2023. Available on-line: www.iea.org/topics/energy-security (access verified on 13/09/2023).

[5] Tarun Kataray, B. Nitesh, Bharath Yarram, Sanyukta Sinha, Erdem Cuce, Saboor Shaik, Pethurajan Vigneshwaran, Abin Roy, Integration of smart grid with renewable energy sources: Opportunities and challenges – A comprehensive review, Sustainable Energy Technol. Assess. 58 (2023) 103363, https://doi.org/10.1016/j.seta.2023.103363. ISSN 2213–1388.

[6] Linas Gelazanskas, Kelum A.A. Gamage, Demand side management in smart grid: A review and proposals for future direction, Sustain. Cities Soc. 11 (2014) 22–30, https://doi.org/10.1016/j.scs.2013.11.001. ISSN 2210-6707.

[7] A. Faruqui, J.H. Chamberlin, Principles and Practices of Demand-Side Management, Electric Power Research Inst No. EPRI-TR-102556; (1993).

[8] K. Abedrabboh, L. Al-Fagih, Applications of mechanism design in market-based demand-side management: A review, Renew. Sustain. Energy Rev. 171 (2023) 113016, https://doi.org/10.1016/j.rser.2022.113016. ISSN 1364–0321.

[9] International Energy Agency. Demand Response. 2023. Available on-line: www.iea.org/energy-system/energy-efficiency-and-demand/demand-response (access verified on 11/09/2023).

[10] C. Silva, P. Faria, Z. Vale, J.M. Corchado, Demand response performance and uncertainty: A systematic literature review, Energ. Strat. Rev. 41 (2022) 100857, https://doi.org/10.1016/j.esr.2022.100857. ISSN 2211-467X.

[11] Sanduni Peiris, Joseph H.K. Lai, Mohan M. Kumaraswamy, Huiying (Cynthia) Hou, Smart retrofitting for existing buildings: State of the art and future research directions, J. Build. Eng. 76 (2023) 107354, https://doi.org/10.1016/j.jobe.2023.107354. ISSN 2352–7102.

[12] International Energy Agency. Buildings. Available on-line: www.iea.org/energy-system/buildings (access verified on 11/09/2023).

[13] European Commission. In focus: Energy efficiency in buildings. 2020. Available on-line: https://commission.europa.eu/news/focus-energy-efficiency-buildings-2020-02-17_en (access verified on 12/09/2023).

[14] International Energy Agency. Heating. 2023. Available on-line: www.iea.org/energy-system/buildings/heating (access verified on 12/09/2023).

[15] Zhengyi Luo, Jinqing Peng, Jingyu Cao, Rongxin Yin, Bin Zou, Yutong Tan, Jinyue Yan, Demand Flexibility of residential buildings: definitions, flexible loads, and quantification methods, Engineering 16 (2022) 123–140, https://doi.org/10.1016/j.eng.2022.01.010. ISSN 2095-8099.

[16] Y. He, H. Zhou, F. Fahimi, Modeling and demand-based control of responsive building envelope with integrated thermal mass and active thermal insulations, Energy Build. 276 (2022) 112495, https://doi.org/10.1016/j.enbuild.2022.112495. ISSN 0378–7788.

[17] María Victoria Gasca, Federico Ibáñez, David Pozo, Flexibility quantification of thermostatically controlled loads for demand response applications, Electr. Pow. Syst. Res. 202 (2022) 107592, https://doi.org/10.1016/j.epsr.2021.107592. ISSN 0378–7796.

[18] Ekrem Tunçbilek, Çağatay Yıldız, Müslüm Arıcı, Zhenjun Ma, Muhammad Bilal Awan, Chapter 5 - Thermal energy storage for enhanced building energy flexibility, Editor(s): Zhenjun Ma, Müslüm Arıcı, Amin Shahsavar, Building Energy Flexibility and Demand Management, Academic Press, 2023, Pages 89-119, ISBN 9780323995887, doi.org/10.1016/B978-0-323-99588-7.00004-3.

[19] H. Zhan, N. Mahyuddin, R.h. Sulaiman, F. Khayatian, Phase change material (PCM) integrations into buildings in hot climates with simulation access for energy performance and thermal comfort: a review, Constr. Build. Mater. 397 (2023) 132312, https://doi.org/10.1016/j.conbuildmat.2023.132312. ISSN 0950–0618.

[20] David Fischer, Hatef Madani, On heat pumps in smart grids: a review, Renew. Sustain. Energy Rev. 70 (2017) 342–357, https://doi.org/10.1016/j.rser.2016.11.182.

[21] Yongbao Chen, Xu Peng, Gu Jiefan, Ferdinand Schmidt, Weilin Li, Measures to improve energy demand flexibility in buildings for demand response (DR): A review, Energ. Buildings 177 (2018) 125–139, https://doi.org/10.1016/j.enbuild.2018.08.003.

[22] Søren Østergaard Jensen, Anna Marszal-Pomianowska, Roberto Lollini, Wilmer Pasut, Armin Knotzer, Peter Engelmann, Anne Stafford, Glenn Reynders, IEA EBC Annex 67 Energy Flexible Buildings, Energ. Buildings 155 (2017) 25–34, https://doi.org/10.1016/j.enbuild.2017.08.044. ISSN 0378-7788.

[23] Vladimir Z. Gjorgievski, Natasa Markovska, Alajdin Abazi, Neven Duić, The potential of power-to-heat demand response to improve the flexibility of the energy system: an empirical review, Renew. Sustain. Energy Rev. 138 (2021) 110489, https://doi.org/10.1016/j.rser.2020.110489. ISSN 1364–0321.

[24] A. Arteconi, A. Mugnini, F. Polonara, Energy flexible buildings: A methodology for rating the flexibility performance of buildings with electric heating and cooling systems, Appl. Energy 251 (2019) 113387, https://doi.org/10.1016/j.apenergy.2019.113387. ISSN 0306–2619.

[25] Glenn Reynders, Rui Amaral Lopes, Anna Marszal-Pomianowska, Daniel Aelenei, João Martins, Dirk Saelens, Energy flexible buildings: an evaluation of definitions

and quantification methodologies applied to thermal storage, Energy Build. 166 (2018) 372–390, https://doi.org/10.1016/j.enbuild.2018.02.040.
[26] F. Pallonetto, M. De Rosa, F. D'Ettorre, D.P. Finn, On the assessment and control optimisation of demand response programs in residential buildings, Renew. Sustain. Energy Rev. 127 (2020) 109861, https://doi.org/10.1016/j.rser.2020.109861.
[27] H. Li, Z. Wang, T. Hong, M.A. Piette, Energy flexibility of residential buildings: a systematic review of characterization and quantification methods and applications, Adv. Appl. Energy 3 (2021) 100054, https://doi.org/10.1016/j.adapen.2021.100054. ISSN 2666–7924.
[28] H. Tang, S. Wang, H. Li, Flexibility categorization, sources, capabilities and technologies for energy-flexible and grid-responsive buildings: State-of-the-art and future perspective, Energy 219 (2021) 119598, https://doi.org/10.1016/j.energy.2020.119598. ISSN 0360–5442.
[29] Rune Grønborg Junker, Armin Ghasem Azar, Rui Amaral Lopes, Karen Byskov Lindberg, Glenn Reynders, Rishi Relan, Henrik Madsen, Characterizing the energy flexibility of buildings and districts, Appl. Energy 225 (2018) 175–182, https://doi.org/10.1016/j.apenergy.2018.05.037.
[30] N. Majdalani, D. Aelenei, R.A. Lopes, C.A.S. Silva, The potential of energy flexibility of space heating and cooling in Portugal, Util. Policy 66 (2020) 101086, https://doi.org/10.1016/j.jup.2020.101086. ISSN 0957–1787.
[31] Glenn Reynders, Jan Diriken, Dirk Saelens, Generic characterization method for energy flexibility: Applied to structural thermal storage in residential buildings, Appl. Energy 198 (2017) 192–202, https://doi.org/10.1016/j.apenergy.2017.04.061.
[32] Hong Tang, Shengwei Wang, Energy flexibility quantification of grid-responsive buildings: Energy flexibility index and assessment of their effectiveness for applications, Energy 221 (2021) 119756, https://doi.org/10.1016/j.energy.2021.119756. ISSN 0360–5442.
[33] Y. Ruan, J. Ma, H.a. Meng, F. Qian, X.u. Tingting, J. Yao, Potential quantification and impact factors analysis of energy flexibility in residential buildings with preheating control strategies, J. Build. Eng. 78 (2023) 107657, https://doi.org/10.1016/j.jobe.2023.107657. ISSN 2352–7102.
[34] Yongbao Chen, Xu Peng, Gu Jiefan, Ferdinand Schmidt, Weilin Li, Measures to improve energy demand flexibility in buildings for demand response (DR): A review, Energ. Buildings 177 (2018) 125–139, https://doi.org/10.1016/j.enbuild.2018.08.003.
[35] H. Li, T. Hong, On data-driven energy flexibility quantification: a framework and case study, Energy Build. 296 (2023) 113381, https://doi.org/10.1016/j.enbuild.2023.11338. ISSN 0378–7788.
[36] J. Zhu, J. Niu, Z. Tian, R. Zhou, C. Ye, Rapid quantification of demand response potential of building HAVC system via data-driven model, Appl. Energy 325 (2022) 119796, https://doi.org/10.1016/j.apenergy.2022.119796. ISSN 0306–2619.
[37] L.u. Fei, Y.u. Zhenyu, Y.u. Zou, X. Yang, Energy flexibility assessment of a zero-energy office building with building thermal mass in short-term demand-side management, Journal of Building Engineering 50 (2022) 104214, https://doi.org/10.1016/j.jobe.2022.104214.
[38] ISO 13786:2017. Thermal performance of building components. Dynamic thermal characteristics. Calculation methods.
[39] Rick Kramer, Jos van Schijndel, Henk Schellen, Simplified thermal and hygric building models: A literature review, Frontiers of Architectural Research 1 (4) (2012) 318–325, https://doi.org/10.1016/j.foar.2012.09.001. ISSN 2095-2635.
[40] Y. Li, Z. O'Neill, L. Zhang, J. Chen, P. Im, J. DeGraw, Grey-box modeling and application for building energy simulations - a critical review, Renew. Sustain. Energy Rev. 146 (2021) 111174, https://doi.org/10.1016/j.rser.2021.111174. ISSN 1364–0321.
[41] Alfonso P. Ramallo-González, Matthew E. Eames, David A. Coley, Lumped parameter models for building thermal modelling: an analytic approach to simplifying complex multi-layered constructions, Energy Build. 60 (2013) 174–184, https://doi.org/10.1016/j.enbuild.2013.01.014. ISSN 0378-7788.
[42] Peder Bacher, Henrik Madsen, Identifying suitable models for the heat dynamics of buildings, Energy Build. 43 (7) (2011) 1511–1522, https://doi.org/10.1016/j.enbuild.2011.02.005. ISSN 0378-7788.
[43] A.P. Ramallo-González, M.E. Eames, S. Natarajan, D. Fosas-de-Pando, D.A. Coley, An analytical heat wave definition based on the impact on buildings and occupants, Energy Build. 216 (2020) 109923, https://doi.org/10.1016/j.enbuild.2020.109923. ISSN 0378–7788.
[44] CT , Micro SCH Acceleration project , Carbon Trust (2011) .
[45] Alice Mugnini, Fabio Polonara, Alessia Arteconi, Energy flexibility curves to characterize the residential space cooling sector: the role of cooling technology and emission system, Energy Build. 253 (2021) 111335, https://doi.org/10.1016/j.enbuild.2021.111335. ISSN 0378-7788.
[46] G. Pernigotto and A. Gasparella. 2018. Classification of European Climates for Building Energy Simulation Analyses, DOI: https://docs.lib.purdue.edu/ihpbc/300/.
[47] Climate.OneBuilding.Org. Available on-line: climate.onebuilding.org/default.html (access verified on 15/09/2023).
[48] S. Huang, S. Katipamula, R. Lutes, Experimental investigation on thermal inertia characterization of commercial buildings for demand response, Energy Build. 252 (2021) 111384, https://doi.org/10.1016/j.enbuild.2021.111384. ISSN 0378–7788.